16. Takahashi Y, Imahori Y, Mineura K (2003) Prognostic and therapeutic indicator of fluoroboronophenylalanine positron emission tomography in patients with gliomas. Clin Cancer Res 9:5888–5895
17. Stupp R, Mason WP, van den Bent MJ, Weller M, Fisher B, Taphoorn MJ, Belanger K, Brandes AA, Marosi C, Bogdahn U, Curschmann J, Janzer RC, Ludwin SK, Gorlia T, Allgeier A, Lacombe D, Cairncross JG, Eisenhauer E, Mirimanoff RO (2005) Radiotherapy plus concomitant and adjuvant temozolomide for glioblastoma. N Engl J Med 352:987–996
18. Gabayan AJ, Green SB, Sanan A, Jenrette J, Schultz C, Papagikos M, Tatter SP, Patel A, Amin P, Lustig R, Bastin KT, Watson G, Burri S, Stea B (2006) GliaSite brachytherapy for treatment of recurrent malignant gliomas: a retrospective multi-institutional analysis. Neurosurgery 58:701–709; discussion 701–709
19. Hermanto U, Frija EK, Lii MJ, Chang EL, Mahajan A, Woo SY (2007) Intensity-modulated radiotherapy (IMRT) and conventional three-dimensional conformal radiotherapy for high-grade gliomas: does IMRT increase the integral dose to normal brain? Int J Radiat Oncol Biol Phys 67:1135–1144
20. Kawabata S, Miyatake S, Kajimoto Y, Kuroda Y, Kuroiwa T, Imahori Y, Kirihata M, Sakurai Y, Kobayashi T, Ono K (2003) The early successful treatment of glioblastoma patients with modified boron neutron capture therapy. Report of two cases. J Neurooncol 65:159–165
21. Miyatake S, Kuroiwa T, Kajimoto Y, Miyashita M, Tanaka H, Tsuji M (2007) Fluorescence of non-neoplastic, MRI-enhancing tissue by 5-aminolevulenic acid: report of 3 cases. Neurosurgery 61:E1101–E1103
22. Sonoda Y, Kumabe T, Takahashi T, Shirane R, Yoshimoto T (1998) Clinical usefulness of 11C-MET PET and 201T1 SPECT for differentiation of recurrent glioma from radiation necrosis. Neurol Med Chir (Tokyo) 38:342–347; discussion 347–348
23. Rock JP, Scarpace L, Hearshen D, Gutierrez J, Fisher JL, Rosenblum M, Mikkelsen T (2004) Associations among magnetic resonance spectroscopy, apparent diffusion coefficients, and image-guided histopathology with special attention to radiation necrosis. Neurosurgery 54:1111–1117; discussion 1117–1119
24. Shankar LK, Hoffman JM, Bacharach S, Graham MM, Karp J, Lammertsma AA, Larson S, Mankoff DA, Siegel BA, Van den Abbeele A, Yap J, Sullivan D (2006) Consensus recommendations for the use of 18F-FDG PET as an indicator of therapeutic response in patients in National Cancer Institute Trials. J Nucl Med 47:1059–1066
25. Meller J, Sahlmann CO, Scheel AK (2007) 18F-FDG PET and PET/CT in fever of unknown origin. J Nucl Med 48:35–45
26. Burger PC, Mahley MS Jr, Dudka L, Vogel FS (1979) The morphologic effects of radiation administered therapeutically for intracranial gliomas: a postmortem study of 25 cases. Cancer 44:1256–1272
27. Wang SX, Boethius J, Ericson K (2006) FDG-PET on irradiated brain tumor: ten years' summary. Acta Radiol 47:85–90
28. Hung GU, Tsai SC, Lin WY (2005) Extraordinarily high F-18 FDG uptake caused by radiation necrosis in a patient with nasopharyngeal carcinoma. Clin Nucl Med 30:558–559
29. Ceyssens S, Van Laere K, de Groot T, Goffin J, Bormans G, Mortelmans L (2006) [11C]methionine PET, histopathology, and survival in primary brain tumors and recurrence. AJNR Am J Neuroradiol 27:1432–1437
30. Tsuyuguchi N, Takami T, Sunada I, Iwai Y, Yamanaka K, Tanaka K, Nishikawa M, Ohata K, Torii K, Morino M, Nishio A, Hara M (2004) Methionine positron emission tomography for differentiation of recurrent brain tumor and radiation necrosis after stereotactic radiosurgery – in malignant glioma. Ann Nucl Med 18:291–296
31. Laverman P, Boerman OC, Corstens FH, Oyen WJ (2002) Fluorinated amino acids for tumour imaging with positron emission tomography. Eur J Nucl Med Mol Imaging 29:681–690
32. Imahori Y, Ueda S, Ohmori Y, Sakae K, Kusuki T, Kobayashi T, Takagaki M, Ono K, Ido T, Fujii R (1998) Positron emission tomography-based boron neutron capture therapy using boronophenylalanine for high-grade gliomas: part I. Clin Cancer Res 4:1825–1832
33. Imahori Y, Ueda S, Ohmori Y, Sakae K, Kusuki T, Kobayashi T, Takagaki M, Ono K, Ido T, Fujii R (1998) Positron emission tomography-based boron neutron capture therapy using boronophenylalanine for high-grade gliomas: part II. Clin Cancer Res 4:1833–1841
34. Joensuu H, Kankaanranta L, Seppala T, Auterinen I, Kallio M, Kulvik M, Laakso J, Vahatalo J, Kortesniemi M, Kotiluoto P, Seren T, Karila J, Brander A, Jarviluoma E, Ryynanen P, Paetau A, Ruokonen I, Minn H, Tenhunen M, Jaaskelainen J, Farkkila M, Savolainen S (2003) Boron neutron capture therapy of brain tumors: clinical trials at the Finnish facility using boronophenylalanine. J Neurooncol 62:123–134

BRAIN RESEARCH 1234 (2008) 172–182

available at www.sciencedirect.com

ScienceDirect

www.elsevier.com/locate/brainres

BRAIN RESEARCH

Research Report

Embryonic neural stem cells transplanted in middle cerebral artery occlusion model of rats demonstrated potent therapeutic effects, compared to adult neural stem cells

Kazuya Takahashi[a], *Takao Yasuhara*[a,*], *Tetsuro Shingo*[a], *Kenichiro Muraoka*[a], *Masahiro Kameda*[a], *Akira Takeuchi*[a], *Akimasa Yano*[a], *Kazuhiko Kurozumi*[a], *Takashi Agari*[a], *Yasuyuki Miyoshi*[a], *Kazushi Kinugasa*[b], *Isao Date*[a]

[a]*Department of Neurological Surgery, Okayama University Graduate School of Medicine, Dentistry and Pharmaceutical Sciences, 2-5-1 Shikata-cho, Okayama, 700-8558, Japan*

[b]*Department of Neurological Surgery, Okayama Rehabilitation Center for Traumatic Apallics, Okayama, Japan*

ARTICLE INFO

Article history:
Accepted 22 July 2008
Available online 30 July 2008

Keywords:
Focal ischemia
Magnetic resonance imaging
Neural stem cell
Neuroprotection
Transplantation

ABSTRACT

Cell therapy using stem cells is awaited by stroke patients with impaired movement and cognitive functions, although intravenous alteplase-administration ameliorated outcomes of patients receiving the therapy within 3 h of onset. In this study, we explored the therapeutic effects of neural progenitor cells (NPC) upon middle cerebral artery occlusion (MCAO) model of rats with exploration of the differences between adult and embryonic NPCs in therapeutic effects. GFP-labeled adult or embryonic NPCs were transplanted for transient MCAO model of rats at 1h after reperfusion. Rats were examined behaviorally using limb placement test, rotarod test and cylinder test with neuroradiological assessment using magnetic resonance imaging (MRI). Consequently after euthanasia, rats were immunohistochemically investigated to explore graft survival and immune reaction. MRI of rats receiving NPCs revealed significant reduction of infarct volumes, compared to vehicle-treated rats with corresponding behavioral amelioration. The transplanted cells were surviving in rats receiving NPCs, although the number of embryonic NPCs was significantly higher than that of adult NPCs. Iba-1-positive inflammatory cells of rats receiving adult NPCs were prominent, compared to those receiving embryonic NPCs, which might be a rationale for the differences between rats receiving adult and embryonic NPCs in the number of surviving NPCs. On the contraries, adult NPCs surely demonstrated therapeutic effects with a few surviving cells, thus indicating that the therapeutic effects might be due to trophic/growth factor-secretion from transplanted NPCs, rather than replacement of damaged host neurons. Therapeutic effects of NPCs for MCAO model of rats were clarified in this study. Transplantation of NPCs

* *Corresponding author*. Fax: +81 86 227 0191.
E-mail address: tyasu37@cc.okayama-u.ac.jp (T. Yasuhara).

Abbreviations: BBB, blood–brain barrier; BDNF, brain-derived neurotrophic factor; BrdU, bromodeoxyuridine; CNPase, 2′, 3′-cyclic nucleotide 3′-phosphodiesterase; CNS, central nervous system; DAPI, 4′, 6-diamidino-2-phenylindole dilactate; Dcx, doublecortin; EGF, epidermal growth factor; FGF, fibroblast growth factor; GDNF, glial cell-line-derived factor; GFAP, glial fibrillary acidic protein; LPT, limb placement test; MCAO, middle cerebral artery occlusion; MSC, mesenchymal stem cell; NGF, nerve growth factor; NPC, neural progenitor cells; SCF, stem cell factor; SVZ, subventricular zone; T2WI, T2-weighted images

0006-8993/$ – see front matter
doi:10.1016/j.brainres.2008.07.086

will be a hopeful strategy for stroke patients, although further studies are required for the patient safety and underlying mechanisms.

1. Introduction

Intravenous administration of alteplase is safe and effective for cerebral infarct when it is used within 3 h of onset (Wahlgren et al., 2007). However, the therapeutic time window is narrow and other therapeutic strategies are awaited especially by stroke patients in subacute and chronic stages. Originally, transplantation therapy was established for the organs with highly proliferative potentials, such as liver transplantation for liver cirrhosis and skin transplantation for burning. Recently, regenerative therapy to the central nervous system (CNS) has reached the level of clinical application by the established methods of isolation and culture of neural stem/progenitor cells. Especially, the cell therapy using neural progenitor cells (NPCs) for stroke to achieve the functional restoration of the damaged neurons might be promising. Stem cells can self-renew and differentiate into multiple lineages suitable for the microenvironment (Akiyama et al., 2001). Furthermore, NPCs might migrate into the damaged area as if it would replace the damaged area

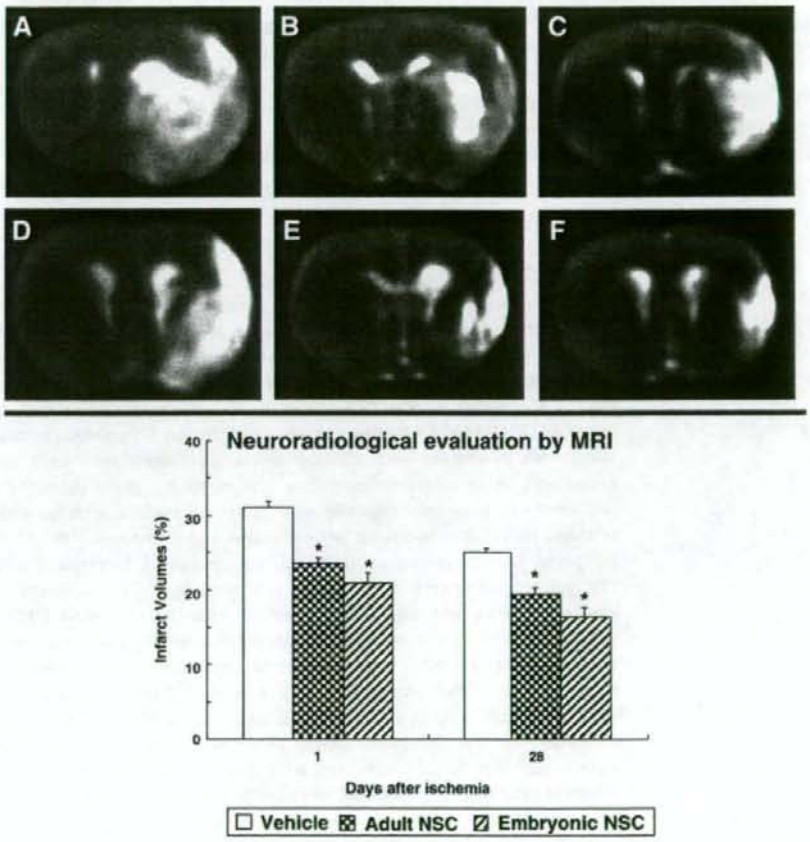

Fig. 1 – Reduced infarct volumes of rats receiving NPCs. Upper column: Representative magnetic T2-weighted images (T2WI) obtained at 1 and 28 days after administration of NPCs or vehicle (vehicle: A and D, adult NPC: B and E, embryonic NPC: C and F) demonstrate that large high-intensity area at 1 day after MCAO reduces at 28 days in all rats. Furthermore, the high-intensity area of rats receiving NPCs is smaller than that of rats in the vehicle group. Lower column: The graph displays that high-intensity area of rats receiving adult or embryonic NPCs is significantly smaller than that of rats in the vehicle group both at 1 and 28 days after transplantation. The effects to reduce infarct volumes of rats receiving embryonic NPCs tend to be more prominent, compared to those of rats receiving adult NPCs, in spite of no significant differences. Data are expressed as mean percentages of infarct volumes ± S.E., relative to the volume of intact hemisphere. ($n=8$ each, $^*p<0.05$ vs. vehicle group).

(Snyder et al., 1997). Recently from several institutes, clinical trials using mesenchymal stem cells (Bang et al., 2005) or human neuronal cells (Kondziolka et al., 2005) for stroke patients were reported with subsequent positive results. However, no clinical trials for stroke patients using NPCs have been reported as a publication. Additionally, some critical issues including the question which origin of NPCs is better, adult or embryonic NPCs, remain to be solved (Prentice and Tarne, 2007; Smith et al., 2007). In this study, the efficacy of NPC-transplantation for cerebral ischemia and the differences between adult and embryonic NPCs were explored with underlying mechanisms.

2. Results

2.1. *GDNF secretion from adult and embryonic NPCs*

The amount of secreted GDNF derived from adult and embryonic NPCs *in vitro* were 77±12 and 89±24 pg/1×10^6 cells/day with no significant difference.

2.2. *Reduced infarct volumes of rats receiving NPC-transplantation*

Infarct volumes of rats receiving adult or embryonic NPCs were significantly smaller than those of rats in the vehicle group both at 1 and 28 days after transplantation (vehicle: 31±0.9 and 25±0.5%; adult NPC: 23.5±0.7 and 19.5±0.8%; embryonic NPC: 21±1.4 and 16±1.4% at 1 and 28 days after middle cerebral artery occlusion (MCAO), respectively; repeated measures of ANOVA, $F_{2,\ 21}=34$, $p<0.0001$ and post-hoc *t*-tests of *p*'s value <0.05 vs. vehicle group, Fig. 1). The effects to reduce infarct volumes of rats receiving embryonic NPCs tends to be more prominent, compared to those receiving adult NPCs, in spite of no significant differences ($p=0.081$). High-intensity signal at 1 day after vehicle infusion significantly reduced at 28 days after transplantation in all groups ($p<0.05$).

2.3. *Ameliorated behavioral scores of rats receiving NPCs*

In all behavioral tests, that is, limb placement test (LPT), rotarod test, and cylinder test, NPC-transplanted rats significantly demonstrated behavioral ameliorations over time, compared to rats in the vehicle group (LPT: vehicle: 3.8±0.5, 6.4±0.6, 7.9±0.5, 8.8±0.6 and 9.5±0.5; adult NPC: 5.1±0.5, 8.0±0.5, 10.3±0.6, 12.4±0.5 and 12.5±0.2; embryonic NPC: 9.5±0.5, 10.3±0.5, 12.3±0.4, 13.1±0.3, 13.8±0.3 at 1, 7, 14, 21 and 28 days after MCAO, respectively. Repeated measures of ANOVA, $F_{2,\ 21}=104$, $p<0.0001$ and post-hoc *t*-tests of *p*'s value <0.05 vs. vehicle group. Time effects were demonstrated in all the comparisons except for Day 21 vs. 28; rotarod test: vehicle: 29±2.4, 46±4.5, 50±4.0, 43±2.4 and 40±4.3%; adult NPC: 60±6.5, 65±8.1, 68±6.5, 73±4.5 and 60±3.3%; embryonic NPC: 77±3.0, 91±2.2, 88±3.6, 89±5.5 and 81±3.1% at±1, 7, 14, 21 and 28 days after MCAO, respectively. Repeated measures of ANOVA, $F_{2,\ 21}=52.8$, $p<0.0001$ and post-hoc *t*-tests of *p*'s value <0.05 vs. vehicle group. Time effects were demonstrated between Day 1 vs. 7, 14 and 21; cylinder test: vehicle: 96±3.1, 76±12, 57±10.7, 47±9.2, and 49±9.2%; adult NPC: 40±1.8, 34±6.2, 41±8.5, 33.8±12 and 17±4.0%; embryonic NPC: 39±8.4, 32±11, 26±7.9, 11±2.2, 10±2.3% at 1, 7, 14, 21 and 28 days after

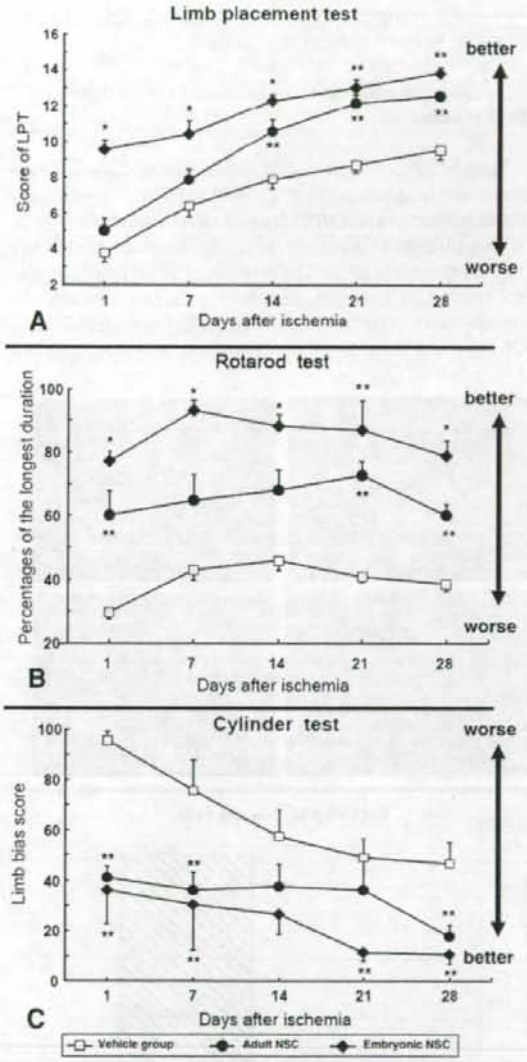

Fig. 2 – Ameliorated behaviors of MCAO rats receiving NPCs. (A) Limb placement test (LPT); (B) Rotarod test; (C) Cylinder test. The scores of LPT, the percentages of rotational durations relative to the pre-MCAO level and the value of cylinder test of rats receiving NPCs are ameliorated at 1, 7, 14, 21 and 28 days after MCAO, compared to that of rats in the vehicle group. Rats receiving embryonic NPCs significantly improve behaviorally in LPT at 1 and 7 days and in rotarod test at 1, 7, 14 and 28 days after MCAO, compared to rats receiving adult NPCs. In cylinder test, there are no significant differences between rats receiving adult and embryonic NPCs. Data are expressed as mean±S.E. *$p<0.05$ vs. adult NPC and vehicle group. **$p<0.05$ vs. vehicle group.

MCAO, respectively. Repeated measures of ANOVA, $F_{2,21}=29$, $p<0.0001$ and post-hoc t-tests of p's value <0.05 vs. vehicle group. Time effects were demonstrated between Day 1 vs. 21 and 28, and Day 7 vs. 28, Fig. 2). Furthermore, in all the behavioral tests, rats receiving embryonic NPCs ameliorated behaviorally, compared to rats receiving adult NPCs with significant differences in some time points.

2.4. *Surviving transplanted NPCs and correlation to infarct volumes*

The surviving cell number of transplanted GFP-positive embryonic NPCs was 267±20 cells/12 sections, significantly more than that of adult NPCs (16±0.5 cells/12 sections, Fig. 3). The transplanted cells mainly resided in the transplanted site in all rats receiving NPCs. The number of adult or embryonic NPCs tended to correlate to infarct volumes in each rat, although there were no significant differences (adult NPC: Y=26.57−0.588*X, R^2=0.535, correlation efficiency: −0.731, p=0.063; embryonic NPC: Y=471.295−0.605*X, R^2=0.481, correlation efficiency: −0.694, p=0.0873, Fig. 4).

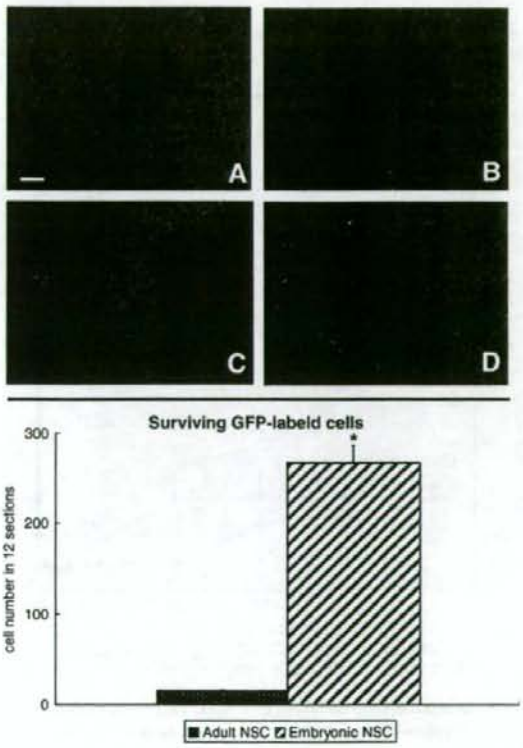

Fig. 3 – Surviving transplanted NPCs resides around the tract and in the ischemic penumbra. Upper column: NeuN (red) immunostaining demonstrates surviving NPCs in the tract (adult NPC, (A) blue-colored nuclear staining; (B) GFP) and in the ischemic penumbra (C) adult NPC; (D) embryonic NPC). Scale bar = 200 μm (A and B), 100 μm (C and D). Lower column: The graph demonstrates that more NPCs significantly survive in rats receiving embryonic NPCs, compared to rats receiving adult NPCs. Data are expressed as mean ± S.E. *p<0.05 vs. adult NPC group.

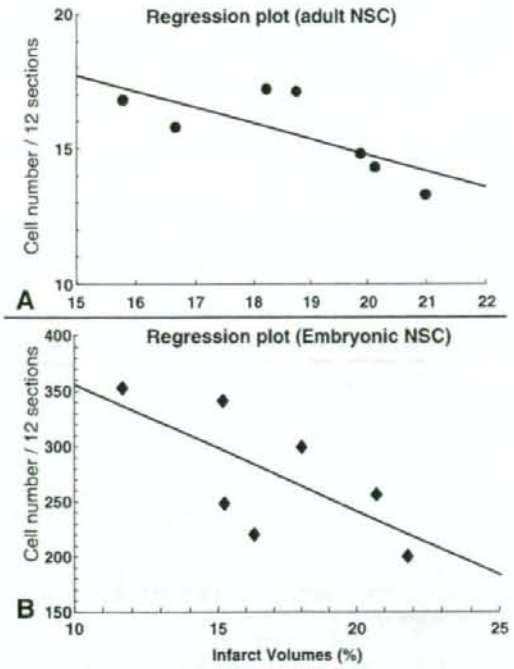

Fig. 4 – The correlation of the surviving NPCs in number and infarct volumes. The graph demonstrates that the number of surviving NPCs in rats with adult NPCs (A) and embryonic NPCs (B) tends to correlates with infarct volumes, respectively.

2.5. *Differentiation of transplanted NPCs*

Both adult and embryonic NPCs differentiated into mature neurons, astrocytes or oligodendrocytes with the expression of each phenotypic marker, that is, neuronal nuclear antigen (NeuN: mature neuronal marker), glial fibrillary acidic protein (GFAP: astrocyte marker), and 2′, 3′-cyclic nucleotide 3′-phosphodiesterase (CNPase: early oligodendrocyte marker, Fig. 5). Over 90% of the transplanted cells differentiated into astrocytes and NeuN-positive mature neurons were recognized in all rats receiving NPCs, although the percentages of neuronal differentiation might be at most 5%. There were no significant differences of neuronal differentiation between adult and embryonic NPC groups.

2.6. *Microglial and astrocytic proliferation induced by transplanted NPCs*

The ratio of reactive cells around the transplanted NPCs relative to that of the vehicle group demonstrated that immune reaction of the host brain receiving embryonic NPCs was weaker than that of adult NPC group (Fig. 6). The ratio of Iba-1-positive area surrounding the transplanted site of rats

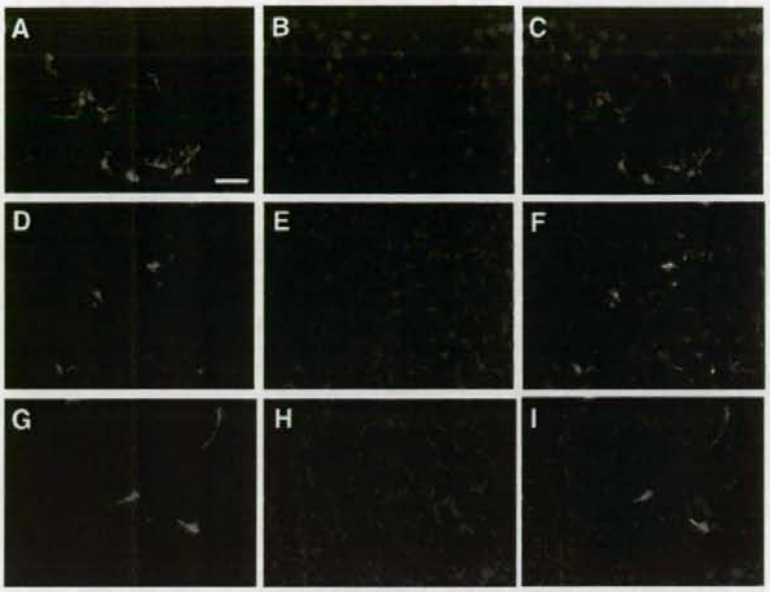

Fig. 5 – Differentiation of NPCs in the ischemic brain. NeuN (A–C), GFAP (D–F), and CNPase (G–I) immunostaining demonstrates that many transplanted cells differentiate into astrocytes, although some cells differentiate into neuronal cells or oligodendrocytes (A, D and G: GFP (green); B, E and H: NeuN, GFAP and CNPase staining (red); C, F and I: merged images). Scale bar: 50 μm.

receiving adult NPCs was 1.7±0.07, which was significantly more than that of rats receiving embryonic NPCs, 1.38±0.084 (Mann–Whitney's U test, $p=0.012$). The ratio of GFAP-positive area of rats receiving adult and embryonic NPCs was 1.3±0.05 and 1.2±0.04 with no significant difference ($p=0.09$).

3. Discussion

Adult or embryonic NPCs were transplanted into transient MCAO model of rats and evaluated neuroradiologically, behaviorally and immunohistochemically in this study to explore the efficacy of NPC-transplantation and the differences between adult and embryo NPCs for cerebral ischemia. Both of adult and embryonic NPCs secreted GDNF. MRI demonstrated that high-intensity area on T2WI reduced at 28 days after MCAO, compared to that obtained at 1 day after MCAO. NPC-transplantation significantly reduced the infarct volumes both at 1 and 28 days after MCAO. NPC-transplantation significantly ameliorated the behavioral scores, compared to that of the vehicle group. Furthermore, embryonic NPCs had intense effects on some behavioral tests, compared to adult NPCs. Accordingly, the number of surviving cells in rats receiving adult NPCs was significantly more than that of rats receiving embryonic NPCs. In each group, the number of surviving NPCs correlated with infarct volumes in spite of no significance. Most transplanted NPCs differentiated into astrocytes, but some differentiated into neurons or oligodendrocytes immunohistochemically in rats receiving NPCs. Iba-1-positive microglia around the tract in rats receiving adult NPCs was more than that in rats receiving embryonic NPCs, demonstrating the inflammatory involvement (Table 1).

3.1. *MRI and infarct volumes*

High-intensity lesion on T2-weighted images (T2WI) after cerebral ischemia was affected by several factors, such as the dynamics of secondary ischemic damage, blood–brain barrier (BBB) disturbances, and the development of vasogenic edema during the reperfusion phase. For example, at 2.5 h from the onset of the ischemic insult, signal intensity on T2WI increased rapidly due to BBB damage and edema formation (Neumann-Haefelin et al., 2000). Thus, the evaluation of the lesion should be carefully performed. On the contraries, normal T2WI might not indicate normal tissue status, as histology and behavior remain abnormal, corresponding to the facts that lasting neurological deficits in some patients with transient ischemia and a normal MRI battery (Sicard et al., 2006; Wegener et al., 2006).

Several studies revealed the relation among infarct volumes detected by MRI, behavioral scores and histological changes. The degree of shift of activation balance toward the non-lesioned hemisphere detected by T2WI at 1 and 14 days after MCAO increased according to the extent of tissue injury and behavioral scores. Additionally, at 3 and 14 days after MCAO, the loss of activation responses in the ipsilateral sensorimotor cortex by functional MRI was related to the size of T2WI high-intensity lesion (Dijkhuizen et al., 2003). Doerfler et al. demonstrated the effectiveness of early craniectomy on

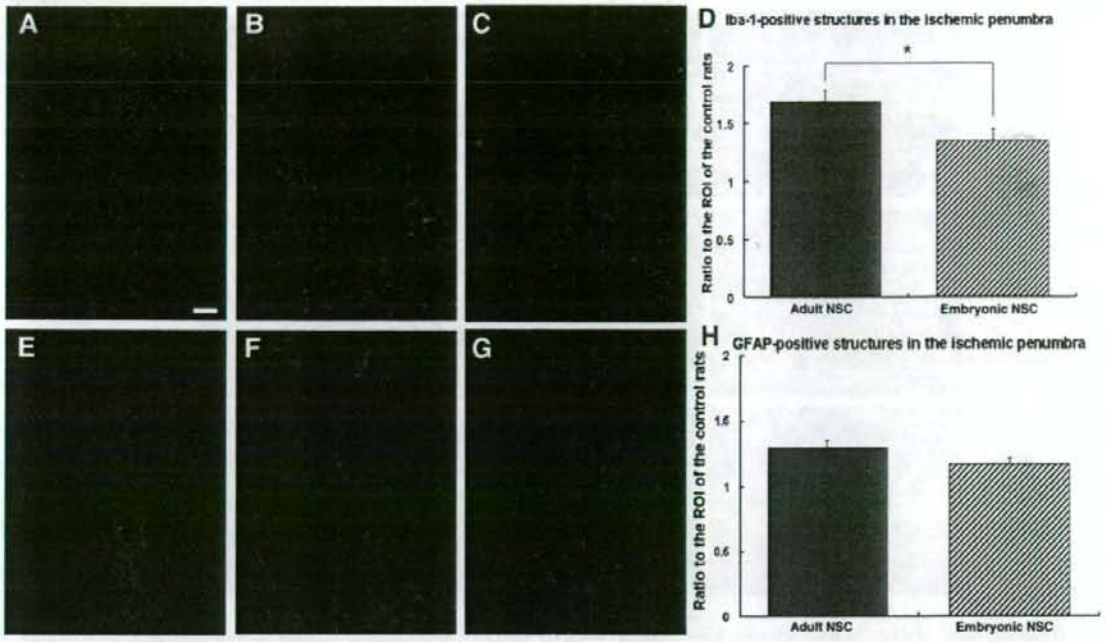

Fig. 6 – Reactive cells around the transplanted NPCs. (A–C) Iba-1 staining around the tract demonstrates the proliferated microglia (A: vehicle, B: adult NPC, C: embryonic NPC). Scale bar: 100 μm. (D) The graph demonstrates that the area of Iba-1-positive structures in rats with adult NPCs is significantly more than that in rats with embryonic NPCs. Data are expressed as mean ratio ± S.E. *$p<0.05$ vs. embryonic NPC group. (E–G) GFAP staining around the tract demonstrates increased astrocytes (E: vehicle, F: adult NPC, G: embryonic NPC). Scale bar: 100 μm. (H) The graph demonstrated that the area of GFAP-positive structures in rats receiving adult NPCs is not significantly different from that in rats receiving embryonic NPCs. Data are expressed as mean ratio ± S.E.

MCAO model of rats to reduce infarct volumes and ameliorate neurological scores (Doerfler et al., 2002). In their study, from 1 to 3 days after MCAO, infarct volumes detected by T2WI correlated well with the histological infarct volumes ($r>0.81$), revealing that the reduction of infarct volumes by T2WI in NPC-transplanted rats might truly corresponded to the reduction of infarct volumes histologically in our study. Other experiments using MRI and histological investigation also demonstrated that histological changes were evident within 12 h, with a significant loss of neurons seen at 7 days after MCAO (Knight et al., 1994).

In our study, the high-intensity area on T2WI reduced at 28 days after MCAO, compared to the area obtained at 1 day after MCAO. The reason of this might include edema, self-renew and atrophy. Correspondingly, doublecortin (Dcx; neuronal progenitor marker)/bromodeoxyuridine (BrdU) or NeuN/BrdU double positive cells were observed in the area possibly with high intensity at 1 day after MCAO and with iso-intensity on T2WI at 28 days after MCAO. Some NPCs from the subventricular zone (SVZ) might migrate to ischemic lesion and differentiate into newborn neurons. Furthermore, behavioral scores, infarct volumes using TTC, NeuN staining and the area of high intensity on T2WI at 14 days after MCAO significantly correlated with each other (in submission to other journal). These data suggest that newborn neurons might at least partially contribute to the spontaneous recovery of the ischemic lesion and behavior.

3.2. *Which NPCs might be better, adult or embryonic?*

In our previous study, cell transplantation might exert therapeutic effects through the replacement of damaged neurons and the secretory functions of neurotrophic factors for neuroprotective effects (Yasuhara et al., 2006). In this study, the amount of GDNF secretion from adult and embryonic NPCs was almost the same. However, more surviving cell number of transplanted embryonic NPCs might secrete more GDNF, compared to adult NPCs with consequent behavioral and immunohistochemical ameliorations in this study.

As a strong therapeutic option at clinical settings in the near future, it might be still controversial whether adult or embryonic NPCs might be suitable for treating diseases (Schallert et al., 2000; Smith et al., 2007). Akiyama et al. demonstrated that transplantation of NPCs into the demyelinated spinal cord resulted in functional remyelination (Akiyama et al., 2001). The potentials of adult and embryonic NPCs might be basically the same, although our previous study revealed that the rate of neural differentiation of adult NPCs might be less than that of embryonic NPCs (Muraoka

et al., 2008). On the other hand, embryonic NPCs, but not adult NPCs usually cause the ethical and political controversy. Autologous adult NPC-transplantation is especially intriguing with no immune rejection as well as no ethical problems (Muraoka et al., 2006). Actually there are over one thousand FDA-approved clinical trials related to adult stem cells in the United States (Prentice and Tarne, 2007). Recently, induced pluripotent stem cells (iPS) cells were established from adult fibroblasts by Oct3/4 and Sox2 gene-transfer (Takahashi and Yamanaka, 2006). However, the proliferating ability of adult stem cells and tumor formation remains still to be solved. In addition, cell-cell interaction of adult and embryonic NPCs might critically differ with consequent neural differentiation and maturation (Karpowicz et al., 2007). The investigations revealing those phenomena and mechanisms should be required.

As described above, autologous adult NPC-transplantation might be hopeful in terms of less immune rejection (Muraoka et al., 2006). Furthermore, there were no significant differences of therapeutic effects between adult and embryonic NPCs engineered to secrete GDNF for PD model of rats (Muraoka et al., 2008). The convincing reason of the different surviving rate and therapeutic effects of transplanted NPCs between the 2 studies might lie in the mechanism that PD model might be less invasive than MCAO model, because of the microcirculatory insufficiency induced by MCAO. In addition, GDNF might exert neuroprotection for transplanted cells and thus help them survive well. Furthermore, the discrepancy might also line in the differences of the efficacy of GFP labeling, viability, vulnerability to the damage on transplantation and responses to inflammatory cells between adult and embryonic NPCs.

3.3. *Therapeutic effects of NPCs*

Goldman proposed 4 representative strategies using stem cells for clinical translation, that is, oligodendrocyte progenitor cells for myelin disorders, phenotypically restricted neuronal progenitor cells to treat diseases of discrete loss of a single neuronal phenotype, such as Parkinson disease, mixed progenitor pools to treat diseases characterized by the loss of several discrete phenotypes, such as spinal cord injury and mobilization of endogenous NPC to restore neuronal cell loss (Goldman, 2005). Apparently, NPC-transplantation will be useful in the near future.

In our previous study, we demonstrated the synergistic effects of NPCs for CNS diseases, that is, replacement of damaged cells and secretion of trophic factors (Yasuhara et al., 2006). Accumulated studies might suggest the reliability of the hypothesis. About the former, human NPCs can migrate, differentiate, and integrate after intravenous transplantation in adult rats with transient forebrain ischemia (Chu et al., 2003) and thus ameliorate sensorimotor deficits in the adult rat brain with experimental focal ischemia (Chu et al., 2004). About the latter mechanism, NPCs might secrete glial cell-line-derived factor (GDNF) and nerve growth factor (NGF) with subsequent neuroprotection for motor neuron (Llado et al., 2004), brain-derived neurotrophic factor (BDNF) with promotion of extensive host axonal growth after spinal cord injury (Lu et al., 2003), and stem cell factor (SCF) with anti-apoptotic effects (Yasuhara et al., 2006) when they are transplanted in the CNS disease model of animals. The concepts of trophic factor-secreting function of NPCs apply to transplantation of mesenchymal stem cells (MSC). MSCs have strong secretory effects of basic fibroblast growth factor (FGF), enhanced neurogenesis, suppressed apoptosis and achieved functional recovery (Chen et al., 2003), although the neuronal differentiation from MSCs was very rare. Gene-transfer to secrete BDNF enhanced neuroprotective potentials (Kurozumi et al., 2004). Other than stem cells, many cells exerted neuroprotective effects, such as umbilical cord blood (Chen et al., 2001) and microglia (Kitamura et al., 2004) with accompanying trophic factor-secretion. In our present study, the overall therapeutic effects of embryonic NPCs might be superior to those of adult NPCs with more surviving cells. However, adult NPCs surely exerted therapeutic effects in spite of a small number of surviving cells, thus indicating underlying trophic factor-secretory effects of transplanted cells with consequent neuroprotective/neurorestorative effects.

3.4. *Differentiation of NPCs*

Since Snyder et al. demonstrated multipotent neural stem/progenitor cells can differentiate for the replacement of damaged neurons undergoing apoptotic degeneration in adult mouse neocortex (Snyder et al., 1997), many reports revealed the potentials of NPC-transplantation. Transplantation of human NPCs might be promising with the synergistic therapeutic effects as described above. Ishibashi et al. reported that transplantation of NPCs derived from human fetus for MCAO rats ameliorated behaviorally and histologically. The grafted NPCs survived with antibodies against NeuN, MAP-2, GFAP or CNPase (Ishibashi et al., 2004), thus, corresponding to our study. In our study, more Iba-1-positive microglia resided around the transplanted site in rats receiving adult NPCs than that in rats receiving embryonic NPC. The ratio of differentiation to neurons, astrocytes, or oligodendrocytes was almost the same in rats with adult and embryonic NPCs, although some report demonstrated that microglia influenced differentiation both of adult and embryonic NPCs (Aarum et al., 2003). The reason of discrepancy might lie in the differences of experimental protocols including timing of cell transplantation and the species of used animals. Additionally, Zhang et al. clarified that adult NPCs had potentials to migrate and differentiate in response to guidance cues within the adult striatum (Zhang et al., 2003), as demonstrated in our study. Yamashita et al. also demonstrated that the SVZ might be an argosy for newly formed neurons (Yamashita et al., 2006), suggesting that adult NPCs from the SVZ used in our study might originally have potentials to differentiate to neurons. Furthermore, the microenvironment of transplanted area might strongly affected the differentiation, migration, and fate (Kelly et al., 2004) through intercellular adhesion molecule (Karpowicz et al., 2007) or neurotrophic factor like GDNF (Paratcha et al., 2006), consistent with our results.

In our study, the therapeutic effects of NPCs were demonstrated for MCAO model of rats behaviorally, neuroradiologically and histologically. The number of surviving cells in rats receiving adult NPCs was significantly fewer than that in rats receiving embryonic NPCs with consequent differences of

therapeutic effects. The surviving cells differentiated into neurons, astrocytes, or oligodendrocytes in all rats receiving NPCs. However on the contraries, the results indicate the synergistic effects of NPC-transplantation, that is, cell replacement and trophic factor-secretion. NPC-transplantation might be hopeful options for stroke patients, although further studies should be performed for establishment of the patient safety.

4. Experimental procedures

4.1. *Animals, experimental groups and outlines of the experiment*

The animal studies were approved by the guidelines of the institutional animal care and use committee of Okayama University. Adult male Wistar rats (Shimizu, Japan) weighing 250–280 g at the beginning of the experiment were used for this study. The rats were housed under a 12 h light–12 h dark cycle with free access to food and water. Animals were divided into 3 experimental groups. Animals in adult and embryonic NPC group ($n=8$ each) were transplanted with NPCs derived from adult and embryonic Wistar rats. The animals in the vehicle group ($n=8$) were injected with 0.01 M phosphate buffered saline (PBS). The transplantation or injection was performed at 1 h after reperfusion after MCAO for 90 min. Between the reperfusion and transplantation, LPT was performed with subsequent no statistical difference of the test scores among the 3 groups. Behavioral tests were performed at 1, 7, 14 and 28 days after MCAO and finally all rats were euthanized at 28 days after MCAO for immunohistochemical investigations.

4.2. *Focal ischemia model*

All rats were anesthetized by a mixture of 1% halothane in nitrous oxide/oxygen (69%/30%) using a face mask. Body temperature was maintained at 37±0.3 °C during the surgical procedures. Focal brain ischemia was induced by the intraluminal suture technique, as previously described (Longa et al., 1989) with a minor modification (Kameda et al., 2007). The midline skin incision was made in the neck with subsequent exploration of the right common carotid artery (CCA), the external carotid artery (ECA) and internal carotid artery (ICA). A 4-0 monofilament nylon suture (17.0–17.5 mm) with the tip polysiloxane-coated (Heraeus Kulzer, Germany) was advanced from the CCA bifurcation until it blocked the origin of the MCA. After 90 min of transient MCAO, animals were re-anesthetized with halothane and reperfused by withdrawal of the nylon thread. Prior to MCAO, a polyethylene tube (SP35, Natsume, Japan) was inserted into the left femoral artery for the monitoring of mean arterial blood pressure (MABP) and arterial blood gas analyses (pH, pO2 and pCO2). MABP and arterial blood samples were analyzed just before and during MCAO.

Table 1 – Summary of the experiments

	Vehicle group	Adult NSC	Embryonic NSC
GDNF secretion	N/A	+	+
Infarct volumes			
at Day 1	–	+	+
at Day 28	–	+	+
Behavioral tests			
Limb placement test	–	+	++
Rotarod test	–	+	++
Cylinder test	–	+	+
Graft survival	N/A	+	++
Neuronal differentiation	N/A	+	+
Microglial proliferation	N/A	++	+
Astrocytic proliferation	N/A	–	–

In order to make it easy to understand the whole data, the data were summarized in this table. N/A: not applicable, –: not significantly effective, +: significantly effective, ++: significantly effective, compared to '+'.

4.3. *Cell preparation*

The isolation and culture of adult NPCs were performed by the method of ours (Muraoka et al., 2006). All Wistar rats were deeply anesthetized with sodium pentobarbital (30 mg/kg, i.p.) and placed in a stereotactic instrument (Narishige, Inc. Tokyo, Japan). A midline skin incision was made in the skull with subsequent drilling for a burr hole. A 16-gauge needle with outer sheath (Terumo, Inc. Tokyo, Japan) attached to a syringe (1.0 ml) was slowly inserted into the cerebrum under mildly negative pressure, the inner needle was withdrawn, and finally brain tissue of the ventricular wall was aspirated through the outer sheath (the coordinates: 1.5 mm anterior and 1.5 mm lateral to the bregma at the depth of 4.0 mm (Paxinos and Watson, 1998)).

Rat embryonic NPCs were also isolated and cultured as previously described (Shingo et al., 2001). Briefly, pregnant Wistar rats were euthanized using over-dosed halothane anesthesia at embryonic day E14.5, the embryos were removed, the ganglionic eminence was dissected from each brain and soaked in PBS with penicillin (50 U/ml).

Then, adult and embryonic NPCs were treated as described previously (Shingo et al., 2001). Briefly, cells from adult rat SVZ were incubated with 1.4 μg/μl trypsin, 0.7 μg/μl hyaluronidase and 0.2 μg/μl kynurenic acid for 15 min at 37 °C with consequent trituration. Then, suspended cells were seeded in Dulbecco's modified Eagle's medium/F12 (Invitrogen Corporation, Grand Island, NY) containing 0.6% glucose, 2 nM NaHCO3, 0.5 mM HEPES, 100 mg/ml human apo-transferrin (Sigma Chemical Co., St. Louis, MO), 60 μM putrescine (Sigma), 20 nM progesterone (Sigma), 30 nM selenium chloride (Sigma), 25 μg/ml human insulin (Sigma), 2 μM L-glutamine, and 20 ng/ml epidermal growth factor (EGF, PeproTech EC, London, UK). Cells were grown in uncoated plastic flasks during the primary culture, as neurospheres. The spheres were subcultured by mechanical dissociation every 10 days and re-seeded on Poly-HEME 2-hydroxyethyl methacrylate, Sigma)-coated flasks as a single cell solution at a density of 1×10^5 cells/ml into the culture media with 20 ng/ml EGF. Neural stem/progenitor cell populations were obtained from neurospheres after 2 passages at 37 °C in a humidified 5% CO_2 atmosphere.

4.4. GFP-gene transfection to adult and embryonic NPCs with adenovirus

As shown in our previous reports (Muraoka et al., 2008), GFP was transferred for the labeling of transplanted cells using adenovirus. Adult and embryonic NPCs were exposed to the infectious viral particles in 40 ml of the culture media at 37 °C for 12 h. Cells were infected with recombinant adenovirus vectors carrying GFP at multiplicity of infection (MOI) of 10^2. Then the cells were washed with the fresh media and cultured with the media without EGF. At 48 h after the gene-transfer, NPCs were re-seeded. GFP-expression was confirmed at 5 days after transfection before transplantation. Finally, the GFP-labeled cell concentration was adjusted to 1.0×10^5 cells/μl using PBS just before transplantation.

4.5. GDNF ELISA analyses

The supernatant of cultured adult and embryonic NPCs were collected for 24 h. GDNF ELISA kits (Progega) were used to quantify the GDNF secretion from NPCS at 1 week after GFP-gene transfection, according to the manufacturer's instruction.

4.6. Transplantation procedure

All Wistar rats were anesthetized with sodium pentobarbital (30 mg/kg, i.p.) and placed in a stereotactic instrument (Narishige, Inc. Tokyo, Japan). A midline skin incision was made in the skull with subsequent drilling for a burr hole. Then 1×10^5 cells (1 μl) of adult NPCs, embryonic NPCs or PBS was injected to the cerebral cortex corresponding to the ischemic penumbra as demonstrated in our previous study (the coordinates: 0 mm anterior and 5.5 mm lateral to the bregma at the depth of 2.3 mm (Kameda et al., 2007; Paxinos and Watson, 1998)) using a Hamilton syringe (26-gauge needle). All surgical procedures were conducted under aseptic conditions.

4.7. MRI studies and measurement of infarct volumes

At 1 and 28 days after MCAO, rats were anesthetized with 30 mg/kg of pentobarbital (i.p.) prior to MRI examinations using a clinical imaging system at 1.5 T (Signa® Advantage MR system: General Electric, Yokogawa, Japan). Continuous, coronal T2WI were obtained using a spin-echo technique (TR=3000, TE=85) from the pole of the frontal lobe to the most caudal portion of the cerebellum. To avoid underestimation due to the brain atrophy in the chronic phase, a "corrected infarct area" (CIA) was calculated as follows, according to (Neumann-Haefelin et al., 2000): CIA=LT −(RT−RI), where LT and RT are the area of the left and right hemisphere, and RI is the high-intensity area of T2WI in square millimeters. In this study, infarct volumes were calculated using CIA and the slice thickness in MRI examinations.

4.8. Behavioral tests

Each rat was subjected to a series of behavioral tests during 28 days after stroke. The tests included (1) the LPT performed before transplantation and at 1, 7, 14, 21, and 28 days after MCAO; (2) the rotarod test and (3) cylinder test both performed at 1, 7, 14, 21, and 28 days after MCAO.

4.8.1. Limb placement test

The LPT was performed to evaluate the degree of hemiparesis. The test included 8 subtests, described by Johansson and Ohlsson (1996). Briefly, the rats' four limbs were evaluated using the top and edges of a counter top. For each subtest, animals received a score of 0: if they were unable to place their limbs; 1: if they displayed partial and/or delayed (more than 2 s) placement of their limbs; and 2: if they exhibited immediate and correct limb placement.

4.8.2. Rotarod test

Rotarod test was also performed to evaluate the degree of hemiparesis and coordinated movements. All rats were trained to stay on the accelerating rotarod (Shinano-Seisaku-syo, Japan) at a constant speed of 8 rpm until they could remain on the rotarod for 100 s before MCAO. Since then, the time they remained on the rotarod which speed was slowly increased from 4 to 40 rpm within 5 min was measured. The data after MCAO were presented as percentage of the longest time on the rotarod of 3 trials compared with the baseline control obtained before MCAO.

4.8.3. Cylinder test

Cylinder test was performed to assess the spontaneous movements, especially focused on the forelimb akinesia. This task was designed by Schallert et al. (2000). For the present study, forelimb-use bias was analyzed the rats' movements while in a transparent Plexiglas cylinder (diameter 18 cm, height 30 cm) for 3-minute intervals. The cylinder was wide enough to allow movement but small enough to encourage rearing and wall exploration. The height of the cylinder disallowed the rat to reach the top edge. Independent vs. combined use of the forelimbs during vertical exploration of the walls was scored as follows. During a rear, the first forelimb placement on the wall was scored as an independent wall movement for that limb. If followed by placement of the other limb on the wall (without first removing the first paw), the movement would be scored a simultaneous limb-use movement. Each subsequent movement along the wall was scored in the same manner. Lateral exploration of the wall by alternating right and left limb placement would result in a series of "simultaneous limb-use" scores, whereas hopping along the wall using 1 limb would result in a series of independent limb-use scores for that limb. Percent-use scores were calculated for (1) movements using the unimpaired limb relative to the total number of movements and (2) movements using the impaired limb relative to the total number of movements. The percent use of the impaired limb was then subtracted from the percent use of the unimpaired limb to create an overall limb-bias score.

4.9. Immunohistochemical investigations

Frozen coronal sections of the brains were cut with a sliding microtome set to 14 μm. Sections including the transplanted site from 1 mm anterior to and 1 mm posterior to the bregma were used for immunohistochemical investigations in each rat.

Double staining of 4′, 6-diamidino-2-phenylindole, dilactate (DAPI, 1:1000, Molecular Probes)/Dcx, DAPI/GFAP, or DAPI/

CNPase was performed to reveal whether cells newly born in the hippocampus differentiated dominantly into neuronal cells, astrocytes, or oligodendrocytes (Yasuhara et al., 2004, 2006). DAPI staining was used for the evaluation of cell viability. From each brain, 12 sections, collected every 154 μm, were washed with PBS and then incubated in guinea pig anti-Dcx (Abcam, MA, USA, 1:200), rabbit anti-GFAP (Chemicon, CA, USA, 1:500) or rabbit anti-CNPase (Abcam, MA, USA, 1:500) with 10% normal goat serum at 4 °C for 18 h. The sections were then washed in PBS 3 times with subsequent incubation in goat anti-rabbit or anti-guinea pig IgG Alexa Fluor 594 (Molecular Probes, 1:1000) for 2 h, washed in 0.01 M PB and finally mounted onto clean glass slides. The slides were cover-slipped using mounting medium (Prolong Antifade Kit, Molecular Probes). Similarly, Iba-1 staining was performed using rabbit anti-IBa-1 antibody (Wako Pure Chemical Industries, Osaka, Japan, 1:100). Control studies included exclusion of primary antibody substituted with 10% normal goat serum in PBS. No immunoreactivity was observed in these controls without GFP-labeled transplanted cells.

4.10. *Quantification using microscope*

GFP-labeled transplanted cells, Dcx-, GFAP-, CNPase-, Iba-1--positive cells were examined using a Zeiss LSM510 confocal microscope (Oberkochen, Germany). Specifically, 12 coronal sections were collected from each rat and the number of GFP-labeled cells was counted. The area of GFAP- and Iba-1-positive structures in each 4 high power fields (HPFs using a 20× objective lens on a Zeiss LSM510 confocal microscope) of the penumbra was measured using Scion Image software and the averages were used for the statistical analyses. In order to explore the differentiation of GFP-labeled transplanted cells, GFAP-, Dcx-, or CNPase-staining were performed with DAPI staining using a 20-power objective lens on a Zeiss LSM510 confocal microscope.

4.11. *Statistical analyses*

Data are presented as the mean±S.E. Data were evaluated statistically using repeated measures of ANOVA for infarct volumes and behavioral tests, Mann–Whitney's *U* test for surviving cell number and GFAP- and Iba-1-density, tests using Pearson's correlation coefficient for the correlation between the cell number and infarct volumes. Statistical significance was preset at $p<0.05$.

Acknowledgments

This work was supported in part by Grants-in-Aid for Scientific Research from the Ministry of Education, Culture, Sports, Science, and Technology, Japan.

REFERENCES

Aarum, J., Sandberg, K., Haeberlein, S.L., Persson, M.A., 2003. Migration and differentiation of neural precursor cells can be directed by microglia. Proc. Natl. Acad. Sci. U. S. A. 100, 15983–15988.

Akiyama, Y., Honmou, O., Kato, T., Uede, T., Hashi, K., Kocsis, J.D., 2001. Transplantation of clonal neural precursor cells derived from adult human brain establishes functional peripheral myelin in the rat spinal cord. Exp. Neurol. 167, 27–39.

Bang, O.Y., Lee, J.S., Lee, P.H., Lee, G., 2005. Autologous mesenchymal stem cell transplantation in stroke patients. Ann. Neurol. 57, 874–882.

Chen, J., Sanberg, P.R., Li, Y., Wang, L., Lu, M., Willing, A.E., Sanchez-Ramos, J., Chopp, M., 2001. Intravenous administration of human umbilical cord blood reduces behavioral deficits after stroke in rats. Stroke 32, 2682–2688.

Chen, J., Li, Y., Katakowski, M., Chen, X., Wang, L., Lu, D., Lu, M., Gautam, S.C., Chopp, M., 2003. Intravenous bone marrow stromal cell therapy reduces apoptosis and promotes endogenous cell proliferation after stroke in female rat. J. Neurosci. Res. 73, 778–786.

Chu, K., Kim, M., Jeong, S.W., Kim, S.U., Yoon, B.W., 2003. Human neural stem cells can migrate, differentiate, and integrate after intravenous transplantation in adult rats with transient forebrain ischemia. Neurosci. Lett. 343, 129–133.

Chu, K., Kim, M., Park, K.I., Jeong, S.W., Park, H.K., Jung, K.H., Lee, S.T., Kang, L., Lee, K., Park, D.K., Kim, S.U., Roh, J.K., 2004. Human neural stem cells improve sensorimotor deficits in the adult rat brain with experimental focal ischemia. Brain Res. 1016, 145–153.

Dijkhuizen, R.M., Singhal, A.B., Mandeville, J.B., Wu, O., Halpern, E.F., Finklestein, S.P., Rosen, B.R., Lo, E.H., 2003. Correlation between brain reorganization, ischemic damage, and neurologic status after transient focal cerebral ischemia in rats: a functional magnetic resonance imaging study. J. Neurosci. 23, 510–517.

Doerfler, A., Engelhorn, T., Heiland, S., Benner, T., Forsting, M., 2002. Perfusion- and diffusion-weighted magnetic resonance imaging for monitoring decompressive craniectomy in animals with experimental hemispheric stroke. J. Neurosurg. 96, 933–940.

Goldman, S., 2005. Stem and progenitor cell-based therapy of the human central nervous system. Nat. Biotechnol. 23, 862–871.

Ishibashi, S., Sakaguchi, M., Kuroiwa, T., Yamasaki, M., Kanemura, Y., Shizuko, I., Shimazaki, T., Onodera, M., Okano, H., Mizusawa, H., 2004. Human neural stem/progenitor cells, expanded in long-term neurosphere culture, promote functional recovery after focal ischemia in Mongolian gerbils. J. Neurosci. Res. 78, 215–223.

Johansson, B.B., Ohlsson, A.L., 1996. Environment, social interaction, and physical activity as determinants of functional outcome after cerebral infarction in the rat. Exp. Neurol. 139, 322–327.

Kameda, M., Shingo, T., Takahashi, K., Muraoka, K., Kurozumi, K., Yasuhara, T., Maruo, T., Tsuboi, T., Uozumi, T., Matsui, T., Miyoshi, Y., Hamada, H., Date, I., 2007. Adult neural stem and progenitor cells modified to secrete GDNF can protect, migrate and integrate after intracerebral transplantation in rats with transient forebrain ischemia. Eur. J. Neurosci. 26, 1462–1478.

Karpowicz, P., Inoue, T., Runciman, S., Deveale, B., Seaberg, R., Gertsenstein, M., Byers, L., Yamanaka, Y., Tondat, S., Slevin, J., Hitoshi, S., Rossant, J., van der Kooy, D., 2007. Adhesion is prerequisite, but alone insufficient, to elicit stem cell pluripotency. J. Neurosci. 27, 5437–5447.

Kelly, S., Bliss, T.M., Shah, A.K., Sun, G.H., Ma, M., Foo, W.C., Masel, J., Yenari, M.A., Weissman, I.L., Uchida, N., Palmer, T., Steinberg, G.K., 2004. Transplanted human fetal neural stem cells survive, migrate, and differentiate in ischemic rat cerebral cortex. Proc. Natl. Acad. Sci. U. S. A. 101, 11839–11844.

Kitamura, Y., Takata, K., Inden, M., Tsuchiya, D., Yanagisawa, D., Nakata, J., Taniguchi, T., 2004. Intracerebroventricular injection

of microglia protects against focal brain ischemia. J. Pharmacol. Sci. 94, 203–206.
Knight, R.A., Dereski, M.O., Helpern, J.A., Ordidge, R.J., Chopp, M., 1994. Magnetic resonance imaging assessment of evolving focal cerebral ischemia. Comparison with histopathology in rats. Stroke 25, 1252–1261 discussion 1261–1252.
Kondziolka, D., Steinberg, G.K., Wechsler, L., Meltzer, C.C., Elder, E., Gebel, J., Decesare, S., Jovin, T., Zafonte, R., Lebowitz, J., Flickinger, J.C., Tong, D., Marks, M.P., Jamieson, C., Luu, D., Bell-Stephens, T., Teraoka, J., 2005. Neurotransplantation for patients with subcortical motor stroke: a phase 2 randomized trial. J. Neurosurg. 103, 38–45.
Kurozumi, K., Nakamura, K., Tamiya, T., Kawano, Y., Kobune, M., Hirai, S., Uchida, H., Sasaki, K., Ito, Y., Kato, K., Honmou, O., Houkin, K., Date, I., Hamada, H., 2004. BDNF gene-modified mesenchymal stem cells promote functional recovery and reduce infarct size in the rat middle cerebral artery occlusion model. Mol. Ther. 9, 189–197.
Llado, J., Haenggeli, C., Maragakis, N.J., Snyder, E.Y., Rothstein, J.D., 2004. Neural stem cells protect against glutamate-induced excitotoxicity and promote survival of injured motor neurons through the secretion of neurotrophic factors. Mol. Cell. Neurosci. 27, 322–331.
Longa, E.Z., Weinstein, P.R., Carlso, N.P., Cummins, R., 1989. Reversible middle cerebral artery occlusion without craniectomy in rats. Stroke. 20, 84–91.
Lu, P., Jones, L.L., Snyder, E.Y., Tuszynski, M.H., 2003. Neural stem cells constitutively secrete neurotrophic factors and promote extensive host axonal growth after spinal cord injury. Exp. Neurol. 181, 115–129.
Muraoka, K., Shingo, T., Yasuhara, T., Kameda, M., Yuan, W., Hayase, H., Matsui, T., Miyoshi, Y., Date, I., 2006. The high integration and differentiation potential of autologous neural stem cell transplantation compared with allogeneic transplantation in adult rat hippocampus. Exp. Neurol. 199, 311–327.
Muraoka, K., Shingo, T., Yasuhara, T., Kameda, M., Yuen, W.J., Uozumi, T., Matsui, T., Miyoshi, Y., Date, I., 2008. Comparison of the therapeutic potential of adult and embryonic neural precursor cells in a rat model of Parkinson disease. J. Neurosurg. 108, 149–159.
Neumann-Haefelin, T., Kastrup, A., de Crespigny, A., Yenari, M.A., Ringer, T., Sun, G.H., Moseley, M.E., 2000. Serial MRI after transient focal cerebral ischemia in rats: dynamics of tissue injury, blood–brain barrier damage, and edema formation. Stroke 31, 1965–1972 discussion 1972–1963.
Paratcha, G., Ibanez, C.F., Ledda, F., 2006. GDNF is a chemoattractant factor for neuronal precursor cells in the rostral migratory stream. Mol. Cell. Neurosci. 31, 505–514.
Paxinos, G., Watson, C., 1998. The Rat Brain in Stereotaxic Coordinates. Academic Press, San Diego.
Prentice, D.A., Tarne, G., 2007. Treating diseases with adult stem cells. Science. 315, 328.
Schallert, T., Fleming, S.M., Leasure, J.L., Tillerson, J.L., Bland, S.T., 2000. CNS plasticity and assessment of forelimb sensorimotor outcome in unilateral rat models of stroke, cortical ablation, parkinsonism and spinal cord injury. Neuropharmacology. 39, 777–787.
Shingo, T., Sorokan, S.T., Shimazaki, T., Weiss, S., 2001. Erythropoietin regulates the in vitro and in vivo production of neuronal progenitors by mammalian forebrain neural stem cells. J. Neurosci. 21, 9733–9743.
Sicard, K.M., Henninger, N., Fisher, M., Duong, T.Q., Ferris, C.F., 2006. Long-term changes of functional MRI-based brain function, behavioral status, and histopathology after transient focal cerebral ischemia in rats. Stroke. 37, 2593–2600.
Smith, S., Neaves, W., Teitelbaum, S., 2007. Adult versus embryonic stem cells: treatments. Science 316, 1422–1423 author reply 1422–1423.
Snyder, E.Y., Yoon, C., Flax, J.D., Macklis, J.D., 1997. Multipotent neural precursors can differentiate toward replacement of neurons undergoing targeted apoptotic degeneration in adult mouse neocortex. Proc. Natl. Acad. Sci. U. S. A. 94, 11663–11668.
Takahashi, K., Yamanaka, S., 2006. Induction of pluripotent stem cells from mouse embryonic and adult fibroblast cultures by defined factors. Cell. 126, 663–676.
Wahlgren, N., Ahmed, N., Davalos, A., Ford, G.A., Grond, M., Hacke, W., Hennerici, M.G., Kaste, M., Kuelkens, S., Larrue, V., Lees, K. R., Roine, R.O., Soinne, L., Toni, D., Vanhooren, G., 2007. Thrombolysis with alteplase for acute ischaemic stroke in the Safe Implementation of Thrombolysis in Stroke-Monitoring Study (SITS-MOST): an observational study. Lancet. 369, 275–282.
Wegener, S., Weber, R., Ramos-Cabrer, P., Uhlenkueken, U., Sprenger, C., Wiedermann, D., Villringer, A., Hoehn, M., 2006. Temporal profile of T2-weighted MRI distinguishes between pannecrosis and selective neuronal death after transient focal cerebral ischemia in the rat. J. Cereb. Blood Flow Metab. 26, 38–47.
Yamashita, T., Ninomiya, M., Hernandez, A.P., Garcia-Verdugo, J.M., Sunabori, T., Sakaguchi, M., Adachi, K., Kojima, T., Hirota, Y., Kawase, T., Araki, N., Abe, K., Okano, H., Sawamoto, K., 2006. Subventricular zone-derived neuroblasts migrate and differentiate into mature neurons in the post-stroke adult striatum. J. Neurosci. 26, 6627–6636.
Yasuhara, T., Shingo, T., Kobayashi, K., Takeuchi, A., Yano, A., Muraoka, K., Matsui, T., Miyoshi, Y., Hamada, H., Date, I., 2004. Neuroprotective effects of vascular endothelial growth factor (VEGF) upon dopaminergic neurons in a rat model of Parkinson's disease. Eur. J. Neurosci. 19, 1494–1504.
Yasuhara, T., Matsukawa, N., Hara, K., Yu, G., Xu, L., Maki, M., Kim, S.U., Borlongan, C.V., 2006. Transplantation of human neural stem cells exerts neuroprotection in a rat model of Parkinson's disease. J. Neurosci. 26, 12497–12511.
Zhang, R.L., Zhang, L., Zhang, Z.G., Morris, D., Jiang, Q., Wang, L., Zhang, L.J., Chopp, M., 2003. Migration and differentiation of adult rat subventricular zone progenitor cells transplanted into the adult rat striatum. Neuroscience 116, 373–382.

Available online at www.sciencedirect.com
ScienceDirect
Neuroscience Research 60 (2008) 114–119
Neuroscience Research
www.elsevier.com/locate/neures

Rapid communication

Involvement of calcineurin in glutamate-induced mitochondrial dynamics in neurons

Xiao-Jian Han [a], Yun-Fei Lu [a], Shun-Ai Li [b], Kazuhito Tomizawa [a], Kohji Takei [b], Masayuki Matsushita [a,c], Hideki Matsui [a,*]

[a] *Department of Physiology, Okayama University Graduate School of Medicine, Dentistry and Pharmaceutical Sciences, 2-5-1 Shikata-cho, Okayama 700-8558, Japan*
[b] *Department of Neuroscience, Okayama University Graduate School of Medicine, Dentistry and Pharmaceutical Sciences, 2-5-1 Shikata-cho, Okayama 700-8558, Japan*
[c] *Mitsubishi Kagaku Institute of Life Sciences, 11 Minamiooya, Machida, Tokyo 194-8511, Japan*

Received 7 June 2007; accepted 27 September 2007
Available online 13 October 2007

Abstract

Alterations in the morphology and movement of mitochondria influence neuronal viability. However, the precise mechanisms of such alterations are unclear. In this study, we showed calcineurin was involved in the regulation of mitochondrial dynamics. Glutamate stimulation inhibited mitochondrial movement and decreased mitochondrial length in neurons. FK506 and cyclosporine A, calcineurin inhibitors, attenuated the effects of glutamate on mitochondrial dynamics. It was also found that glutamate treatment dephosphorylated, a proapoptotic protein, Bad and promoted its translocation to mitochondria in neurons via calcineurin. These results provide important new insights into intracellular signaling pathways that regulate mitochondrial dynamics and neuronal cell death.

Keywords: Neuronal cell death; Mitochondria; Calcineurin; Calcium; NMDA; Neural excitation; Bad

Mitochondria are involved in a variety of cellular processes, including survival, proliferation, and apoptosis (Shaw and Nunnari, 2002; Fannjiang et al., 2004; Szabadkai et al., 2004; Karbowski et al., 2002), and are dynamic organelles, which move in a cell and frequently undergo fission and fusion (Bereiter-Hahn and Voth, 1994; Rube and van der Bliek, 2004). Under normal physiological conditions, mitochondrial fission and fusion are balanced, and mitochondria maintain a typical thread-like or tubular shape in cells. In neurons, mitochondrial trafficking to pre- and post-synaptic sites is likely to play an important role in control of basal synaptic transmission and synaptic plasticity (Tang and Zucker, 1997; Li et al., 2004). Mitochondrial movement and morphological changes in dendrites are regulated by synaptic activity, while mitochondrial movement in axons responds to changes in axonal outgrowth (Chada and Hollenbeck, 2003; Ruthel and Hollenbeck, 2003; Li et al., 2004). The movement of mitochondria in dendrites can be inhibited in response to glutamate, a process that involves NMDA receptors (Barsoum et al., 2006; Rintoul et al., 2003). However, the precise molecular mechanism downstream of NMDA receptors is unclear.

In the present study, we first examined the effect of glutamate on mitochondrial movement and morphology in primary hippocampal neurons. To label mitochondria, neurons were transfected with pDsRed2-Mito (Clontech), which is a mammalian expression vector that encodes the fluorescent protein DsRed2 tagged with the mitochondrial targeting sequence from subunit VIII of human cytochrome *c* oxidase. Time-lapse imaging of mitochondria was performed automatically with a selected interval using a Zeiss Axiovert 200 inverted fluorescence microscope. Mitochondrial movement was evaluated by analyzing the pDsRed2-Mito signal as detailed previously (Rintoul et al., 2003). Briefly, pixel intensities in successive images at 10-s intervals were subtracted (Fig. 1a). Movement event for each pixel was registered if there was a change in pixel fluorescence between successive fields. Pixel intensity differences between six sequential images were averaged. The pixel area of the image

* Corresponding author. Tel.: +81 86 235 7105; fax: +81 86 235 7111.
E-mail address: matsuihi@cc.okayama-u.ac.jp (H. Matsui).

0168-0102/$ – see front matter
doi:10.1016/j.neures.2007.09.012

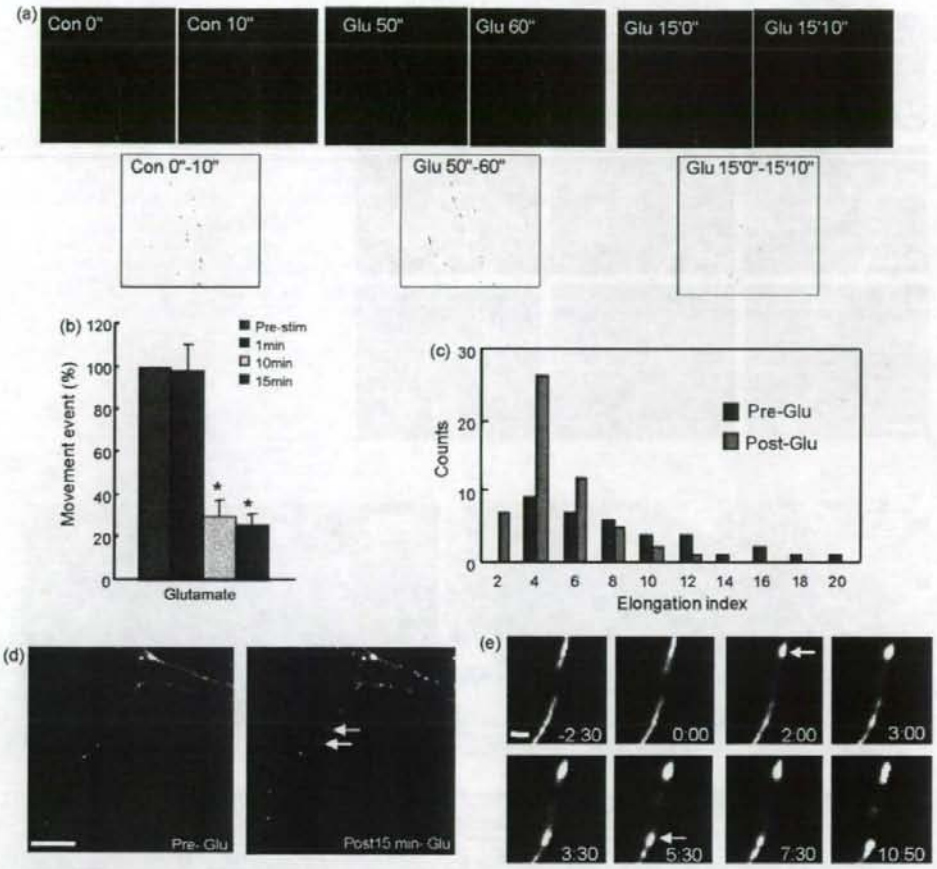

Fig. 1. The effect of glutamate on mitochondrial dynamics in neurons. Neurons (10 DIV) were transfected with pDsRed2-Mito and then (at 11 DIV) treated with 100 μM glutamate for 15 min. Mitochondrial movement and morphology were analyzed by time-lapse imaging. (a) Measurement of mitochondrial movement. The upper sets of panels show the mito-DsRed images. The lower sets of panels show the image subtraction between the indicated 10 s intervals. (b) Summary of glutamate-induced changes in mitochondrial movement. The value from each time point was normalized to that prior to glutamate treatment (pre-Stim). Data are from seven cells in seven different culture dishes. $^*P < 0.001$. (c) Example of histogram showing mitochondrial length pre- or post-glutamate treatment. The elongation index is the square of the longest length divided by the area of each mitochondrion. (d) The thread-like mitochondria were changed to become shorter and round-shaped. Arrows show the glutamate-induced mitochondrial morphological changes. Scale bar, 10 μm. (e) Higher magnification shows the changes of mitochondria induced by glutamate. Shorter and rounder mitochondria are indicated by the white arrows. Scale bar, 1 μm; time in min is indicated at the bottom of each panel. Scale bar, 1 μm.

was normalized to the total mitochondrial pixel area before subtraction. Morphological changes of mitochondria were evaluated by the elongation index, which was calculated as the square of the longest length divided by the area; i.e., when the elongation index was bigger, mitochondria were longer. Analysis was performed using AquaCosmos software (Hamamatsu Photonics). The effect of glutamate on mitochondrial movement and length in hippocampal neurons was examined (Fig. 1b and c). An onset of cessation of mitochondrial movement was usually observed from 5 to 10 min after glutamate application (mitochondrial movement was reduced to 98.8% at 1 min, 30.2% at 10 min and 26.3% at 15 min compared to the pre-glutamate movement, Fig. 1b). The change of movement was accompanied by a decrease of mitochondrial length (Fig. 1c). Glutamate stimulation increased the number of mitochondria with small elongation index (Fig. 1c). The thread-like mitochondria in dendrites became shorter after glutamate treatment, and time-lapse imaging showed that mitochondria were notably round-shaped after glutamate treatment (Fig. 1d and e). Moreover, the morphological changes of mitochondrial were also observed after treatment with various concentrations (10–500 μM) of glutamate. Mitochondrial shape could recover 3 h after 50 and 100 μM glutamate treatment, whereas the morphological changes of mitochondria was irreversible when neurons were treated with 500 μM glutamate (Fig. 2a). Mitochondrial morphology after glutamate treatment was further assessed by electron microscopic analysis. Mitochondria in dendrites from control neurons were rod-shaped and their cristae were clear. After treatment with glutamate, mitochondria were changed into round-shaped structures with highly condensed cristae stacked on top of each other (Fig. 2b).

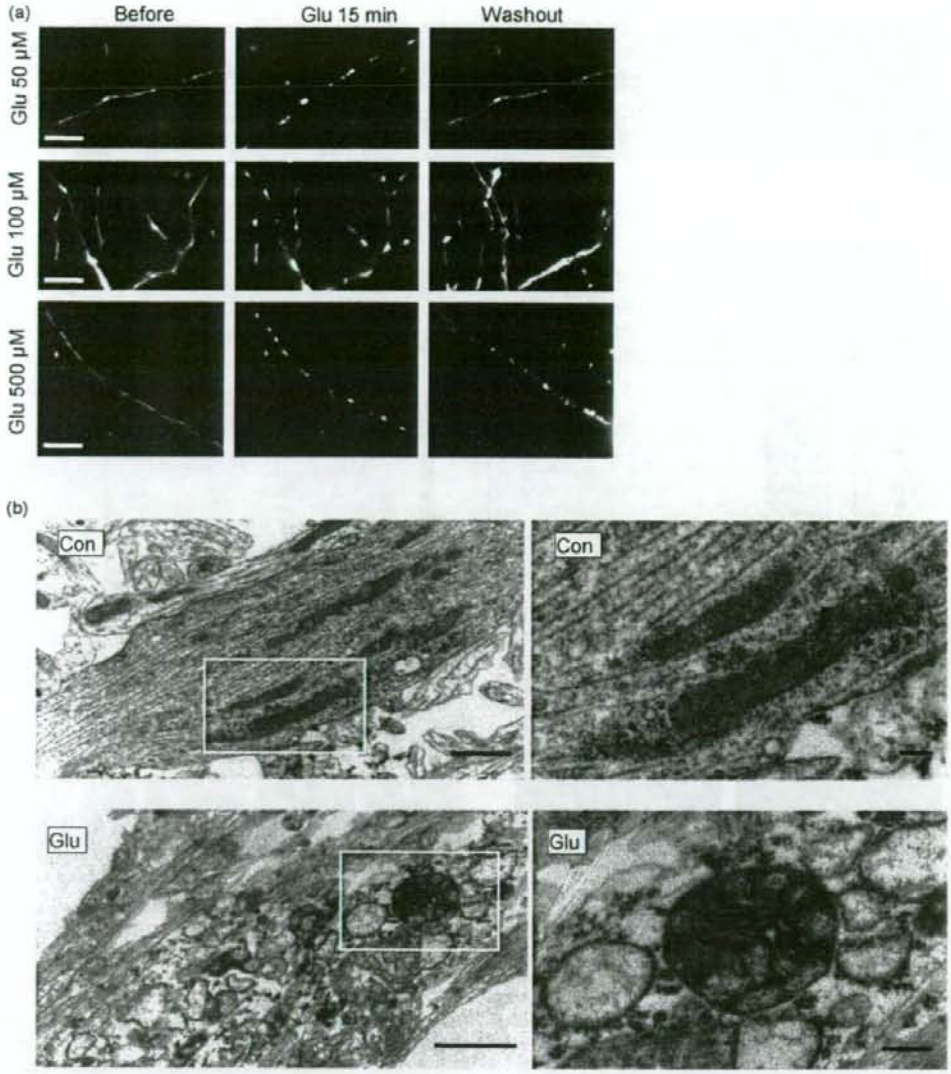

Fig. 2. The recovery of mitochondrial shape after glutamate and ultrastructural changes of mitochondria induced by glutamate. (a) Recovery of mitochondrial morphology after glutamate. Neurons (11 DIV) were treated with 100 μM glutamate for 15 min post-transfection with pDsRed2-Mito (at 10 DIV) and mitochondrial fluorescence was analyzed by time-lapse imaging. Mitochondria were analyzed prior (pre-Glu) to addition of various concentrations of glutamate as indicated, and 15 min after glutamate addition. After 15 min of stimulation, glutamate was removed by exchange of medium, and mitochondria were imaged again after 3 h. Scale bar, 10 μm. (b) Ultrastructure of mitochondria was analyzed by electron microscopy. The upper two panels show examples of mitochondria from control neurons. The lower two panels show examples of mitochondria in neurons following treatment with 100 μM glutamate for 15 min. Micrographs at low and high magnification are shown in the left and right column, respectively. Scale bar, 1.0 μm on the left and 200 nm on the right.

Previous studies have shown that NMDA receptors are involved in glutamate-induced changes in mitochondrial movement and shape (Rintoul et al., 2003; Barsoum et al., 2006). In agreement with the previous studies, the effects of glutamate on the movement and morphological changes of mitochondria were attenuated by APV (50 μM), an NMDA receptor antagonist (Fig. 3c). To investigate the events downstream from the NMDA receptor in glutamate-induced morphological changes of mitochondria, we measured the intracellular Ca^{2+} level following glutamate treatment. Ca^{2+} imaging was performed as detailed previously (Saheki et al., 2005). The intracellular Ca^{2+} change was indicated as the ratio of emitted fluorescence at 340 nm and 380 nm excitations. Glutamate application triggered a rapid increase in intracellular Ca^{2+}. The increased Ca^{2+} was sustained 30 min after glutamate exposure (Fig. 3a). To further investigate Ca^{2+}-dependent signaling pathways that act downstream of NMDA receptors, we examined the effects of Ca^{2+}/calmodulin-dependent kinase or phosphatase inhibitors. KN93, an inhibitor of Ca^{2+}/calmodulin-dependent protein kinases (CaMKs), had no effect

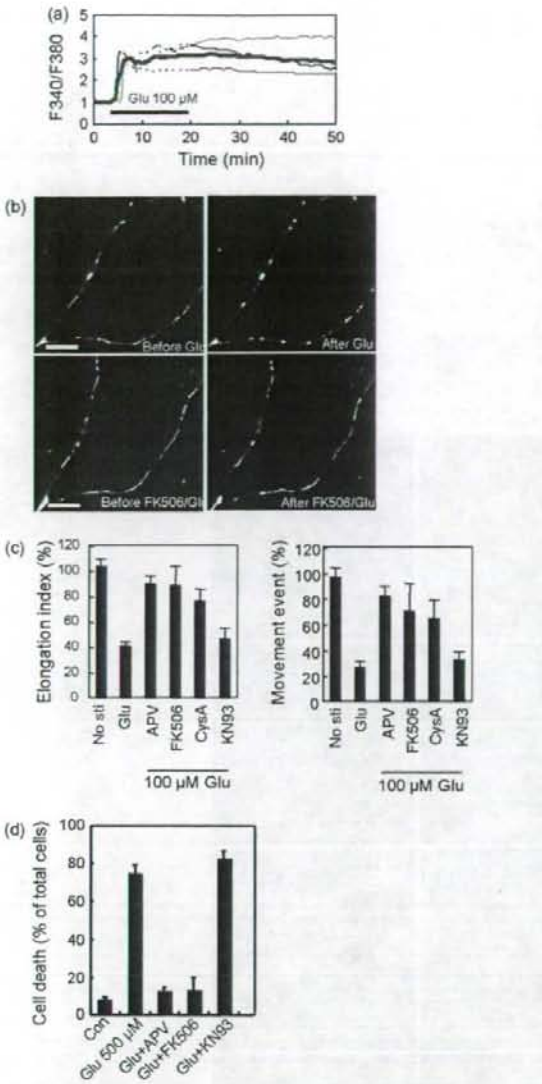

Fig. 3. Involvement of calcineurin in the effect of glutamate on mitochondria and neuronal viability. (a) Intracellular Ca^{2+} levels were measured in hippocampal neurons (12 DIV) in response to treatment with 100 μM glutamate. The graph shows the normalized ratio of F340/F380 in four different neurons (thin lines) and the average value (bold line). Glutamate treatment induced a prolonged elevation of intracellular Ca^{2+} after washout of glutamate. (b) Neurons (10 DIV) were transfected with pDsRed2-Mito and analyzed by time-lapse imaging. Cells (11 DIV) were incubated with 100 μM glutamate for 15 min (upper panels) or pretreated for 30 min with 1 μM FK506 prior to glutamate treatment (lower panels). Scale bar, 10 μm. (c) Mitochondrial length or movement was measured for neurons that were either untreated (no sti), incubated with 100 μM glutamate for 15 min (Glu), or pretreated with the indicated pharmacological agents for 30 min prior to glutamate: APV (50 μM), FK506 (1 μM), cyclosporin A (CysA, 10 μM) or KN93 (20 μM). The results are the averages from five experiments. (d) Neuronal viability after glutamate treatment. Hippocampal neurons were either untreated (Con), exposed to 500 μM glutamate for 15 min, or pretreated with the indicated pharmacological agents for 30 min prior to 500 μM glutamate; APV (50 μM), FK506 (1 μM), cyclosporin A (CysA, 10 μM) or KN93 (20 μM). Twenty-four hours after exposure to glutamate, cultures were stained with MAP2 antibody and Hoechst 33258. The neurons with condensed Hoechst 33258 staining were counted as dead cells. Data were obtained from at least five visual fields under a 20× objective from three experiments under each condition.

on glutamate-induced changes in mitochondrial movement or morphology, whereas FK506 and cyclosporin A, potent inhibitor of the Ca^{2+}/calmodulin-dependent protein phosphatase, calcineurin, significantly attenuated the effects of glutamate on mitochondrial movement and length (Fig. 3b and c). These results suggest that calcineurin is involved in glutamate-induced mitochondrial movement and morphological changes in neurons.

A number of previous studies have shown that calcineurin is involved in excitatory neuronal cell death (Wu et al., 2005). Calcineurin is constitutively activated following its cleavage by calpain during neuroexcitotoxic stimuli such as glutamate application, resulting in the induction of neuronal cell death (Wu et al., 2004). In the present study, 500 μM glutamate, which irreversibly altered mitochondrial movement and morphology, induced neuronal cell death. APV and FK506 blocked glutamate-induced neuronal cell death, whereas KN93 had no effect on the neuronal cell death (Fig. 3d). A low concentration (50 μM) of glutamate, which reversibly affected mitochondrial movement and morphology, did not induce neuronal cell death (data not shown). A previous study showed that glutamate-induced ultrastructural changes of mitochondria, resulting in an increase in cytochrome *c* release from mitochondria (Zieminska et al., 2006). Release of cytochrome *c* from the mitochondria to the cytoplasm induces neuronal cell death through the activation of caspase (Polster and Fiskum, 2004). Moreover, cytochrome *c* release is regulated by members of Bcl-2 family (Kluck et al., 1997; Yang et al., 1997). Bad is a proapoptotic member of the Bcl-2 family that can displace Bax from Bcl-2 and Bcl-xL, resulting cell death (Yang et al., 1995). Under non-apoptotic conditions, Bad is maintained in an inactive phosphorylated state by serine/threonine kinases, such as Akt, mitochondria-anchored PKA (Datta et al., 1997; Harada et al., 1999), which has been shown to inhibit cytochrome *c* release (Kennedy et al., 1999). In apoptotic stimulus, Bad is dephosphorylated, dissociated from 14-3-3, and translocates to mitochondria. To investigate the signaling pathways that act downstream of calcineurin in glutamate-induced dynamic changes of mitochondria and neuronal cell death, we examined the phosphorylation level and localization of Bad following glutamate treatment and the effects of calcineurin inhibitors. The phosphorylation level of Bad was detected by Western blotting analysis using the phospho-specific antibodies. Glutamate treatment reduced the phosphorylation of Bad (both pS112 and pS136-Bad) compared with control. Pretreatment with FK506 and cyclosporin A inhibited glutamate-induced dephosphorylation of Bad at both sites (Fig. 4a). The localization of Bad in respond to glutamate was examined using immunofluorescence analysis. In untreated neurons, Bad was mostly diffused. In contrast, glutamate treatment-induced punctate Bad immunostaining in neurons and the punctate Bad immunostaining was colocalized with

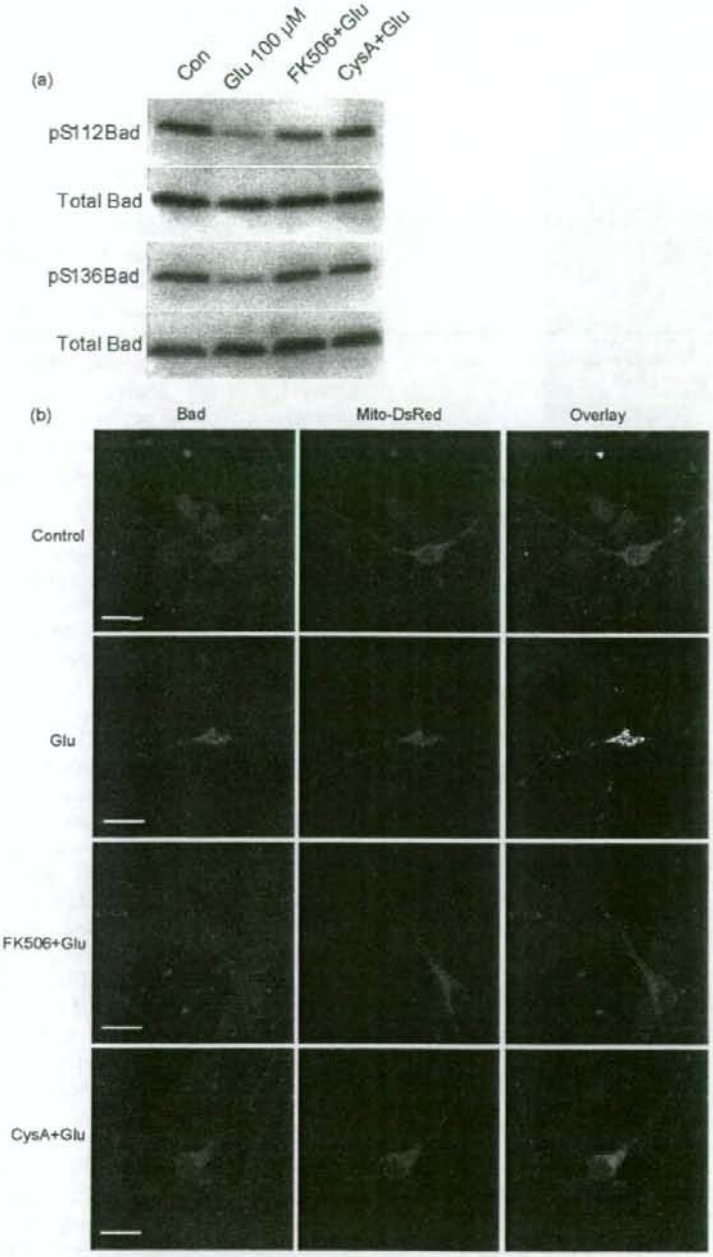

Fig. 4. Calcineurin dephosphorylates Bad and promotes its translocation to mitochondria after glutamate exposure. (a) Dephosphorylation of Bad by calcineurin. Hippocampal neurons were either untreated (Con), exposed to 100 μM glutamate for 15 min, or pretreated with FK506 (1 μM) or cyclosporin A (CysA, 10 μM) for 30 min prior to glutamate. Then neurons were lysed in lysis buffer A (20 mM Tris, pH 7.4, 150 mM NaCl, 10 mM sodium orthovanadate, 20 mM sodium fluoride, 0.25 M sucrose, 1 mM dithiothreitol, 0.5% Tween 20) supplemented with protease inhibitors: 1 mM phenylmethylsulfonyl fluoride, leupeptin (5 μg/ml), pepstatin A (5 μg/ml), aprotinin (5 ug/ml). The lysates were subjected to 15% SDS–PAGE and immunoblot analysis with phosphorylation state-dependent pS112-Bad, pS136-Bad antibodies (cell signaling) or phosphorylation state-independent Bad antibody (BD Biosciences). (b) Localization of Bad in neurons after glutamate treatment. Neurons (10 DIV) were transfected with pDsRed2-Mito. Cells (11 DIV) were either untreated (Con), exposed to 100 μM glutamate for 15 min, or pretreated with FK506 (1 μM) or cyclosporin A (CysA, 10 μM) for 30 min prior to glutamate. After glutamate treatment, cells were fixed in 4% paraformaldehyde and incubated overnight at 4 °C with phosphorylation state-independent Bad antibody. Detection was performed using second antibody conjugated to FITC. Immunofluorescence and mitochondria were examined using an Olympus laser confocal microscope (Fluoview 300, Olympus). Scale bar, 20 μm.

mitochondria. Pretreatment with calcineurin inhibitors FK506 or cyclosporin A blocked glutamate-induced Bad translocation to mitochondria (Fig. 4b). These results indicate that glutamate stimulation triggers Bad translocation to mitochondria through calcienurin-mediated dephosphorylation of Bad. Although there is no direct evidence showing that Bad dephosphorylation regulates mitochondrial dynamics, some clues imply such possibility. For example, the dephosphorylated Bad displaces Bax from Bcl-2 and Bcl-xL in apoptotic stimulus (Yang et al., 1995). Bax is involved in apoptotic fragmentation of mitochondria (Karbowski et al., 2002). Taking together, it highly implies the involvement of Bad in glutamate-induced dynamic changes of mitochondria. Moreover, previous studies have shown cyclosporine A has protective effect on mitochondrial permeability transition and prevents cell death (Pastorino et al., 1993; Friberg et al., 1998). These results suggest the immunosuppressants protect neuronal cell death through inhibition of glutamate-induced changes in mitochondrial dynamics and mitochondrial permeability transition.

In conclusion, glutamate inhibited mitochondrial movement and decreased mitochondrial length in primary hippocampal neurons. Inhibition of calcineurin attenuated the effects of glutamate on mitochondrial movement and morphology. Calcineurin was also found to dephosphorylate Bad and promote its translocation to mitochondria in neurons after glutamate treatment. These results suggest that calcineurin plays a crucial role in the regulation of mitochondrial dynamics and neuronal cell death.

Acknowledgment

This work was supported by a Grant-in-Aid for Scientific Research from the Ministry of Education, Science, Sports and Culture of Japan.

References

Barsoum, M.J., Yuan, H., Gerencser, A.A., Liot, G., Kushnareva, Y., Graber, S., Kovacs, I., Lee, W.D., Waggoner, J., Cui, J., White, A.D., Bossy, B., Martinou, J.C., Youle, R.J., Lipton, S.A., Ellisman, M.H., Perkins, G.A., Bossy-Wetzel, E., 2006. Nitric oxide-induced mitochondrial fission is regulated by dynamin-related GTPases in neurons. EMBO J. 25, 3900–3911.

Bereiter-Hahn, J., Voth, M., 1994. Dynamics of mitochondria in living cells: shape changes, dislocations, fusion, and fission of mitochondria. Microsc. Res. Tech. 27, 198–219.

Chada, S.R., Hollenbeck, P.J., 2003. Mitochondrial movement and positioning in axons: the role of growth factor signaling. J. Exp. Biol. 206, 1985–1992.

Datta, S.R., Dudek, H., Tao, X., Masters, S., Fu, H., Gotoh, Y., Greenberg, M.E., 1997. Akt phosphorylation of BAD couples survival signals to the cell-intrinsic death machinery. Cell 91, 231–241.

Fannjiang, Y., Cheng, W.C., Lee, S.J., Qi, B., Pevsner, J., McCaffery, J.M., Hill, R.B., Basanez, G., Hardwick, J.M., 2004. Mitochondrial fission proteins regulate programmed cell death in yeast. Genes Dev. 18, 2785–2797.

Friberg, H., Ferrand-Drake, M., Bengtsson, F., Halestrap, A.P., Wieloch, T., 1998. Cyclosporin A, but not FK 506, protects mitochondria and neurons against hypoglycemic damage and implicates the mitochondrial permeability transition in cell death. J. Neurosci. 18, 5151–5159.

Harada, H., Becknell, B., Wilm, M., Mann, M., Huang, L.J., Taylor, S.S., Scott, J.D., Korsmeyer, S.J., 1999. Phosphorylation and inactivation of BAD by mitochondria-anchored protein kinase A. Mol. Cell. 3, 413–422.

Karbowski, M., Lee, Y.J., Gaume, B., Jeong, S.Y., Frank, S., Nechushtan, A., Santel, A., Fuller, M., Smith, C.L., Youle, R.J., 2002. Spatial and temporal association of Bax with mitochondrial fission sites, Drp1, and Mfn2 during apoptosis. J. Cell Biol. 159, 931–938.

Kennedy, S.G., Kandel, E.S., Cross, T.K., Hay, N., 1999. Akt/Protein kinase B inhibits cell death by preventing the release of cytochrome *c* from mitochondria. Mol. Cell Biol. 19, 5800–5810.

Kluck, R.M., Bossy-Wetzel, E., Green, D.R., Newmeyer, D.D., 1997. The release of cytochrome *c* from mitochondria: a primary site for Bcl-2 regulation of apoptosis. Science 275, 1132–1136.

Li, Z., Okamoto, K., Hayashi, Y., Sheng, M., 2004. The importance of dendritic mitochondria in the morphogenesis and plasticity of spines and synapses. Cell 119, 873–887.

Pastorino, J.G., Snyder, J.W., Serroni, A., Hoek, J.B., Farber, J.L., 1993. Cyclosporin and carnitine prevent the anoxic death of cultured hepatocytes by inhibiting the mitochondrial permeability transition. J. Biol. Chem. 268, 13791–13798.

Polster, B.M., Fiskum, G., 2004. Mitochondrial mechanisms of neural cell apoptosis. J. Neurochem. 90, 1281–1289.

Rintoul, G.L., Filiano, A.J., Brocard, J.B., Kress, G.J., Reynolds, I.J., 2003. Glutamate decreases mitochondrial length and movement in primary forebrain neurons. J. Neurosci. 23, 7881–7888.

Rube, D.A., van der Bliek, A.M., 2004. Mitochondrial morphology is dynamic and varied. Mol. Cell. Biochem. 256–257, 331–339.

Ruthel, G., Hollenbeck, P.J., 2003. Response of mitochondrial traffic to axon determination and differential branch growth. J. Neurosci. 23, 8618–8624.

Saheki, Y., Li, S.T., Matsushita, M., Wu, Y.M., Cai, W.H., Wei, F.Y., Lu, Y.F., Moriwaki, A., Tomizawa, K., Matsui, H., 2005. A new approach to inhibiting astrocytic IP3-induced intracellular calcium increase in an astrocyte-neuron co-culture system. Brain Res. 1055, 196–201.

Shaw, J.M., Nunnari, J., 2002. Mitochondrial dynamics and division in budding yeast. Trends Cell Biol. 12, 178–184.

Szabadkai, G., Simoni, A.M., Chami, M., Wieckowski, M.R., Youle, R.J., Rizzuto, R., 2004. Drp-1-dependent division of the mitochondrial network blocks intraorganellar Ca^{2+} waves and protects against Ca^{2+}-mediated apoptosis. Mol. Cell. 16, 59–68.

Tang, Y., Zucker, R., 1997. Mitochondrial involvement in post-tetanic potentiation of synaptic transmission. Neuron 18, 483–491.

Wu, H.Y., Tomizawa, K., Oda, Y., Wei, F.Y., Lu, Y.F., Matsushita, M., Li, S.T., Moriwaki, A., Matsui, H., 2004. Critical role of calpain-mediated cleavage of calcineurin in excitotoxic neurodegeneration. J. Biol. Chem. 279, 4929–4940.

Wu, H.Y., Yuen, E.Y., Lu, Y.F., Matsushita, M., Matsui, H., Yan, Z., Tomizawa, K., 2005. Regulation of *N*-methyl-D-aspartate receptors by calpain in cortical neurons. J. Biol. Chem. 280, 21588–21593.

Yang, E., Zha, J., Jockel, J., Biose, L.H., Thompson, C.B., Korsmeyer, S.J., 1995. Bad, a heterodimeric partner for Bcl-XL and Bcl-2, displaces Bax and promotes cell death. Cell 80, 285–291.

Yang, J., Liu, X., Bhalla, K., Kim, C.N., Ibrado, A.M., Cai, J., Peng, T.I., Jones, D.P., Wang, X., 1997. Prevention of apoptosis by Bcl-2: release of cytochrome *c* from mitochondria blocked. Science 275, 1129–1132.

Zieminska, E., Matyja, E., Kozlowska, H., Stafiej, A., Lazarewicz, J.W., 2006. Excitotoxic neuronal injury in acute homocysteine neurotoxicity: role of calcium and mitochondrial alterations. Neurochem. Int. 48, 491–497.

Published August 11, 2008

CaM kinase Iα–induced phosphorylation of Drp1 regulates mitochondrial morphology

Xiao-Jian Han,[1] Yun-Fei Lu,[1] Shun-Ai Li,[2] Taku Kaitsuka,[4] Yasufumi Sato,[4] Kazuhito Tomizawa,[1] Angus C. Nairn,[3] Kohji Takei,[2] Hideki Matsui,[1] and Masayuki Matsushita[1,4]

[1]Department of Physiology and [2]Department of Neuroscience, Okayama University Graduate School of Medicine and Dentistry, Okayama 700-8558, Japan
[3]Department of Psychiatry, Yale University School of Medicine, New Haven, CT 06508
[4]Mitsubishi Kagaku Institute of Life Sciences, Machida, Tokyo 194-8511, Japan

Mitochondria are dynamic organelles that frequently move, divide, and fuse with one another to maintain their architecture and functions. However, the signaling mechanisms involved in these processes are still not well characterized. In this study, we analyze mitochondrial dynamics and morphology in neurons. Using time-lapse imaging, we find that Ca^{2+} influx through voltage-dependent Ca^{2+} channels (VDCCs) causes a rapid halt in mitochondrial movement and induces mitochondrial fission. VDCC-associated Ca^{2+} signaling stimulates phosphorylation of dynamin-related protein 1 (Drp1) at serine 600 via activation of Ca^{2+}/calmodulin-dependent protein kinase Iα (CaMKIα). In neurons and HeLa cells, phosphorylation of Drp1 at serine 600 is associated with an increase in Drp1 translocation to mitochondria, whereas in vitro, phosphorylation of Drp1 results in an increase in its affinity for Fis1. CaMKIα is a widely expressed protein kinase, suggesting that Ca^{2+} is likely to be functionally important in the control of mitochondrial dynamics through regulation of Drp1 phosphorylation in neurons and other cell types.

Introduction

Mitochondria play an essential function in cells through the production of energy and the ability to regulate intracellular Ca^{2+}. As such, they are involved in a variety of cellular processes, including survival, proliferation, and apoptosis (Kroemer and Reed, 2000; Shaw and Nunnari, 2002; Fannjiang et al., 2004; Oakes and Korsmeyer, 2004; Szabadkai et al., 2004; Youle and Karbowski, 2005; Karbowski et al., 2006). Mitochondria are also dynamic organelles and move through the cell with frequent fission and fusion processes that influence their morphology (Bereiter-Hahn and Voth, 1994; Rube and van der Bliek, 2004; Chan, 2006).

Recent studies have shed light on the molecular mechanisms involved in mitochondrial fission and fusion. In mammalian cells, mitochondrial fusion is regulated by Fzo1, OPA1, and Mgm1 (Bossy-Wetzel et al., 2003; Lee et al., 2004). In contrast, dynamin-related protein 1 (Drp1), Fis1, and possibly other proteins such as MTP18 play an important role in mitochondrial fission (Stojanovski et al., 2004; Tondera et al., 2005; Yu et al., 2005). A critical role is played by the Drp1, which translocates to mitochondria and forms a complex with Fis1 on the mitochondrial surface. There, Drp1's GTPase activity is coupled to outer membrane scission (Yoon et al., 2001; Barsoum et al., 2006). Mitochondrial fission is likely to be similar to the process involved in plasma membrane endocytosis mediated by the GTPase activity of dynamin, such as in synaptic vesicle endocytosis (Takei et al., 1995). Recent studies suggest that posttranslational modifications including phosphorylation, ubiquitination, and SUMOylation are likely involved in the control of mitochondrial fission (Cerveny et al., 2007; Detmer and Chan, 2007). However, it is still unclear how extracellular stimuli might modulate intracellular signaling processes to control mitochondrial dynamics and morphology.

In neurons, mitochondrial trafficking to pre- and postsynaptic sites is likely to play an important role in control of basal synaptic transmission and plasticity (Tang and Zucker, 1997; Li et al., 2004). In dendrites, mitochondrial movement and morphology

Correspondence to Masayuki Matsushita: masayuki@mitils.jp

Abbreviations used in this paper: ANOVA, analysis of variance; CaMK, Ca^{2+}/calmodulin-dependent protein kinase; CaMKIα-CA, constitutively active CaMKIα; CaMKIα-DN, dominant-negative CaMKIα; DIV, days in vitro; Drp1, dynamin-related protein 1; GED, GTPase effector domain; VDCC, voltage-dependent Ca^{2+} channel.

The online version of this article contains supplemental material.

The Rockefeller University Press $30.00
J. Cell Biol. Vol. 182 No. 3 573–585
www.jcb.org/cgi/doi/10.1083/jcb.200802164

Supplemental Material can be found at:
http://jcb.rupress.org/cgi/content/full/jcb.200802164/DC1

Published August 11, 2008

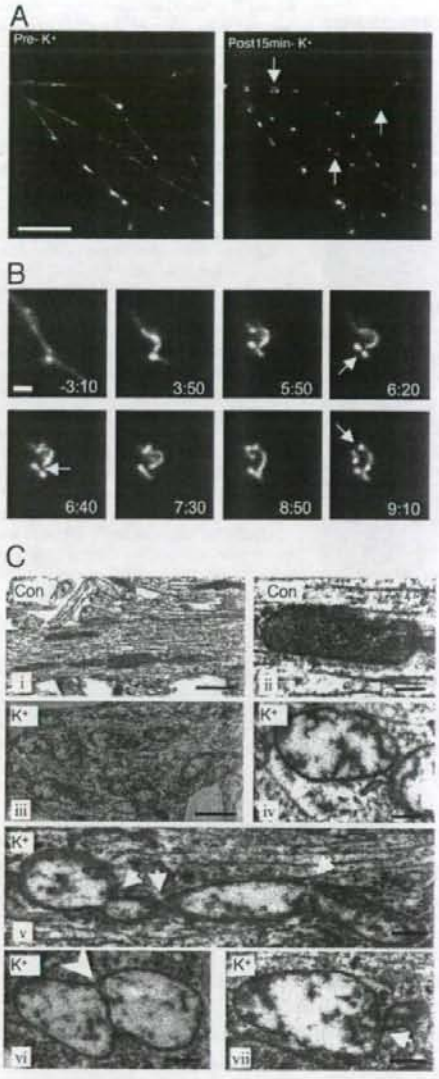

Figure 1. **Effects of high K⁺ on mitochondrial dynamics and morphology in neurons.** (A) Neurons (10 DIV) were transfected with pDsRed2-Mito to label mitochondria. Neurons (at 11 DIV) were then treated with 45 mM K⁺ for 15 min, and mitochondrial fluorescence was analyzed by time-lapse imaging. Arrows show ringlike mitochondria formation in dendrites. Bar, 10 µm. (B) Higher magnification in dendrites show details of ringlike mitochondrial formation induced by treatment with 45 mM K⁺. Arrows show mitochondrial fission. Time in minutes after application of high K⁺ is indicated at the bottom of each panel. Bar, 1 µm. (C) Ultrastructure of mitochondria analyzed by electron microscopy. Panels i and ii show examples of mitochondria from control neurons. The remaining panels (iii–vii) show examples of mitochondria in neurons treated with 45 mM K⁺ for 15 min. (ii) Mitochondria in dendrites from control neurons were rod shaped, and their cristae were clear. (iii–vii) Mitochondria from neurons treated with 45 mM K⁺ formed clusters that exhibited less electron-dense matrices and contained less cristae. (v–vii) 45-mM K⁺ treatment caused mitochondrial fission. Arrows in v–vii show connections between dividing mitochondria. The dividing mitochondria shared continuous outer membrane with separate inner membranes (arrowhead in vi). Bars: (i and iii) 1 µm; (ii and iv–vii) 200 nm.

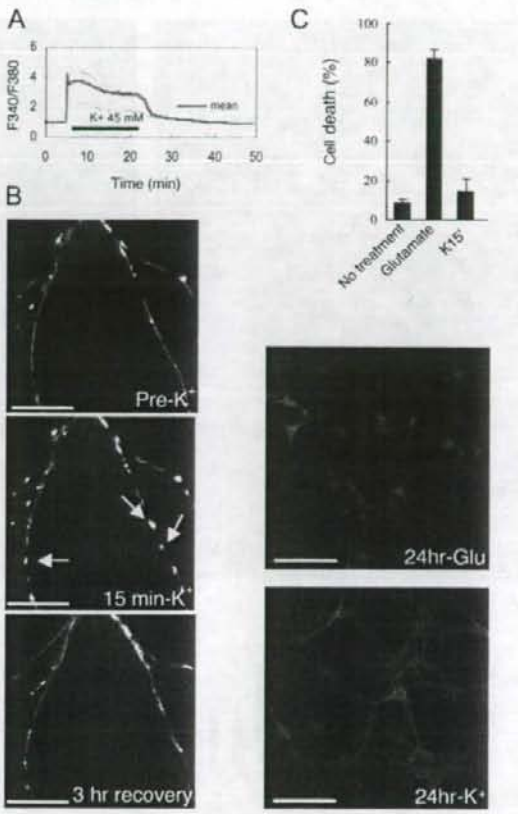

Figure 2. **High K⁺ induces elevation in intracellular Ca^{2+} and reversible changes in mitochondrial morphology.** (A) Intracellular Ca^{2+} level was measured in hippocampal neurons (12 DIV) in response to treatment with 45 mM K⁺. Graphs show normalized ratios of F340/F380 in four different neurons (thin lines) and the mean value (bold line). (B) Neurons transfected with pDsRed2-Mito were analyzed before addition of 45 mM K⁺ and 15 min after treatment with high K⁺. Arrows show ringlike mitochondria formations. After 15 min, 45 mM K⁺ was removed by exchange of media, and mitochondria were imaged after 3 h. The same result was obtained in three separate experiments ($n = 3$). Bars, 10 µm. (C) Neurons (12 DIV) were untreated or treated for 15 min with 500 µM glutamate or 45 mM K⁺. After the 15-min treatment, the media was replaced by conditioned medium from 10-d-old neuronal cultures. 24 h later, cell death was measured by Hoechst 33258 and MAP2 staining. Data were obtained from at least five visual fields under a 20× objective from at least three independent experiments for each group. Error bars indicate SEM in each group. Bars, 40 µm.

are regulated by synaptic activity, whereas in axons, mitochondrial movement responds to changes in axonal outgrowth (Chada and Hollenbeck, 2003; Ruthel and Hollenbeck, 2003; Li et al., 2004). Mitochondrial movement and morphology are also regulated by nitric oxide, and alterations in mitochondrial morphology may play a role in apoptosis (Barsoum et al., 2006; Wasiak et al., 2007). Although mitochondrial movement and fission/fusion play critical functional roles in neurons, it is unclear how these changes in mitochondrial morphology and movement are coupled to alterations in synaptic activity.

In the present study, we find that intracellular signaling associated with activation of voltage-dependent Ca^{2+} channels (VDCCs) regulates mitochondrial dynamics and morphology in